Climate
of the Past

Open Access

Modulation of Late Cretaceous and Cenozoic climate by variable drawdown of atmospheric pCO$_2$ from weathering of basaltic provinces on continents drifting through the equatorial humid belt

D. V. Kent[*,1,2] **and G. Muttoni**[3,4]

[1]Department of Earth and Planetary Sciences, Rutgers University, Piscataway, NJ 08854, USA
[2]Lamont–Doherty Earth Observatory of Columbia University, Palisades, NY 10964, USA
[3]Department of Earth Sciences, University of Milan, via Mangiagalli 34, 20133 Milan, Italy
[4]ALP – Alpine Laboratory of Paleomagnetism, via Madonna dei Boschi 76, 12016 Peveragno (CN), Italy
[*]*Invited contribution by D. V. Kent, one of the EGU Petrus Peregrinus Medal winners 2006.*

Correspondence to: D. V. Kent (dvk@rutgers.edu)

Abstract. The small reservoir of carbon dioxide in the atmosphere (pCO$_2$) that modulates climate through the greenhouse effect reflects a delicate balance between large fluxes of sources and sinks. The major long-term source of CO$_2$ is global outgassing from sea-floor spreading, subduction, hotspot activity, and metamorphism; the ultimate sink is through weathering of continental silicates and deposition of carbonates. Most carbon cycle models are driven by changes in the source flux scaled to variable rates of ocean floor production, but ocean floor production may not be distinguishable from being steady since 180 Ma. We evaluate potential changes in sources and sinks of CO$_2$ for the past 120 Ma in a paleogeographic context. Our new calculations show that decarbonation of pelagic sediments by Tethyan subduction contributed only modestly to generally high pCO$_2$ levels from the Late Cretaceous until the early Eocene, and thus shutdown of this CO$_2$ source with the collision of India and Asia at the early Eocene climate optimum at around 50 Ma was inadequate to account for the large and prolonged decrease in pCO$_2$ that eventually allowed the growth of significant Antarctic ice sheets by around 34 Ma. Instead, variation in area of continental basalt terranes in the equatorial humid belt (5° S–5° N) seems to be a dominant factor controlling how much CO$_2$ is retained in the atmosphere via the silicate weathering feedback. The arrival of the highly weatherable Deccan Traps in the equatorial humid belt at around 50 Ma was decisive in initiating the long-term slide to lower atmospheric pCO$_2$, which was pushed further down by the emplacement of the 30 Ma Ethiopian Traps near the equator and the southerly tectonic extrusion of SE Asia, an arc terrane that presently is estimated to account for 1/4 of CO$_2$ consumption from all basaltic provinces that account for $\sim$ 1/3 of the total CO$_2$ consumption by continental silicate weathering (Dessert et al., 2003). A negative climate-feedback mechanism that (usually) inhibits the complete collapse of atmospheric pCO$_2$ is the accelerating formation of thick cation-deficient soils that retard chemical weathering of the underlying bedrock. Nevertheless, equatorial climate seems to be relatively insensitive to pCO$_2$ greenhouse forcing and thus with availability of some rejuvenating relief as in arc terranes or thick basaltic provinces, silicate weathering in this venue is not subject to a strong negative feedback, providing an avenue for ice ages. The safety valve that prevents excessive atmospheric pCO$_2$ levels is the triggering of silicate weathering of continental areas and basaltic provinces in the temperate humid belt. Excess organic carbon burial seems to have played a negligible role in atmospheric pCO$_2$ over the Late Cretaceous and Cenozoic.

1 Introduction

Deep water temperatures determined from the continuous benthic oxygen isotope record (Cramer et al., 2009, 2011; Miller et al., 2005b; Zachos et al., 2001) (Fig. 1a) document
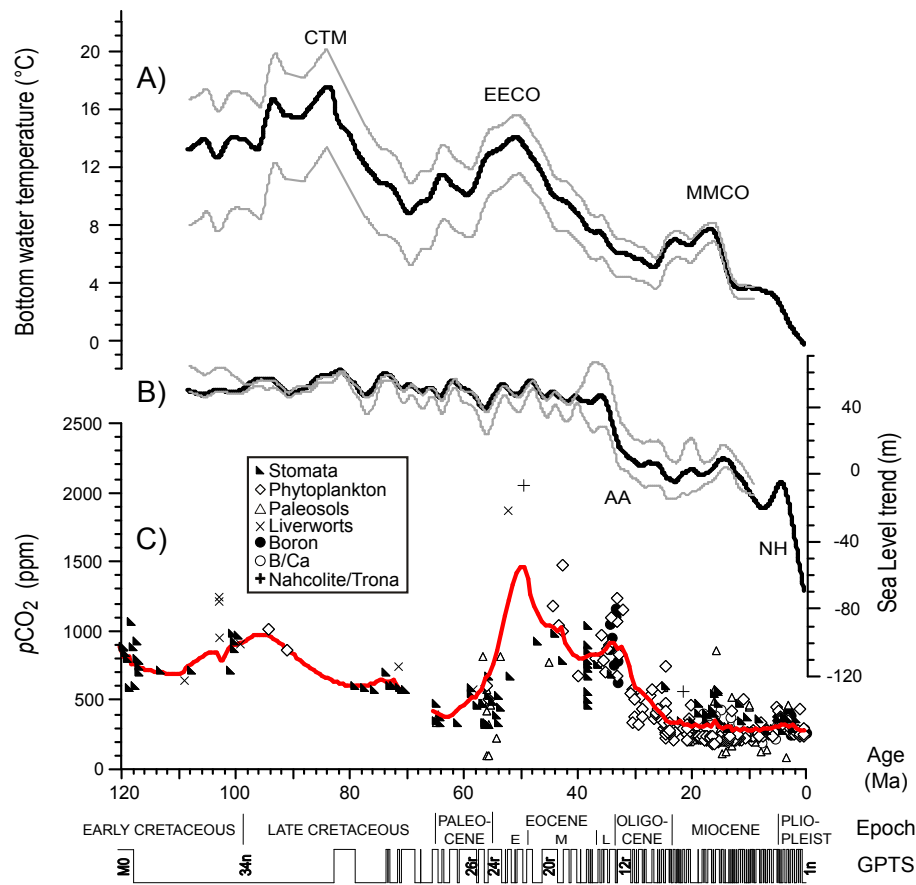
Fig. 1. Bottom water temperatures **(A)** and reconstructed sea levels **(B)** since the Early Cretaceous (Cramer et al., 2011) smoothed to emphasize variations on > 5 Myr timescales. CTM is Cretaceous thermal maximum, EECO is early Eocene climatic optimum, and MMCO is middle Miocene climatic optimum; AA is sea-level drop at the inception of Antarctic ice sheets, and NH is sea-level drop at the inception of Northern Hemisphere ice sheets. **(C)** Atmospheric pCO_2 estimates from various proxies from compilation of Royer (2010) for pre-70 Ma interval (except paleosol estimates, which are highly scattered and have not been plotted) and of Beerling and Royer (2011) for post-70 Ma interval. Simple smoothing functions have been fit (heavy curved line) through the mean pCO_2 estimates provided in the compilations. Ages and epochs registered to GPTS (geomagnetic polarity time scale) of Cande and Kent (1995).

that global climate over the past 120 Myr experienced extremes ranging from equable polar climates with bottom water temperatures over 15 °C during the Cretaceous Thermal Maximum (CTM $\sim$ 90 Ma; Wilson et al., 2002) and the early Eocene climatic optimum (EECO, $\sim$ 50 Ma) to a cooling trend during the Middle and Late Eocene with a major sea level fall (Fig. 1b) at around the Eocene–Oligocene boundary ($\sim$ 34 Ma), marking the inception of major polar (Antarctic) ice sheets.

The equable conditions at the CTM and especially the EECO are associated with warmer global (polar and tropical) sea surface temperatures (Pearson et al., 2001, 2007) that most likely resulted from an enhanced greenhouse effect due to higher atmospheric pCO_2 concentrations as inferred from various proxies (Fig. 1c; see review with references in Beerling and Royer, 2011; Royer, 2010). These high pCO_2 levels have been conventionally attributed to higher rates of ocean crust production and associated increased CO_2 outgassing

(Berner et al., 1983), for example, a presumed pulse of increased global sea-floor spreading and the emplacement of the North Atlantic igneous province at the EECO (Miller et al., 2005a; Rea et al., 1990; Thomas and Bralower, 2005; Zachos et al., 2001). Decreasing pCO_2 levels (Pagani et al., 2005, 2011) and the coincident cooling trend that followed the EECO could then be due to reduced outgassing flux from lower global ocean floor production rates that eventually led to a major buildup of Antarctic ice sheets at around the Eocene–Oligocene boundary (DeConto and Pollard, 2003), whose precise timing may have been influenced by openings of Southern Ocean gateways (Kennett, 1977; Livermore et al., 2007; Stickley et al., 2004).

A spreading rate-dependent CO_2 outgassing factor (Berner, 1994; Berner et al., 1983; Engebretson et al., 1992) is intuitively appealing and usually regarded as the most important parameter driving variations in pCO_2 in the current generation of carbon cycling models (Berner, 2004) but

there are conflicting estimates of global ocean floor production rates. For example, Muller et al. (2008) and Seton et al. (2009) postulate high production in the Late Cretaceous and decreasing production in the Cenozoic, whereas Cogné and Humler (2004, 2006) show high production earlier in the Cretaceous, reduced production in the Late Cretaceous, and increasing production over the Cenozoic. Provocatively, Rowley (2002) showed that the observed area-age versus age distribution of oceanic crust does not require substantial production rate changes since the breakup of Pangea at 180 Ma; the fact that more than 50 % of oceanic lithosphere younger than 55.7 Ma (70 % younger than $\sim$ 89 Ma, 85 % younger than $\sim$ 120 Ma) has already been removed by subduction means that reconstructions of oceanic lithosphere history are invariably based on substantial and often poorly constrained extrapolations (Rowley, 2008). Moreover, carbon uptake by oceanic crust may tend to cancel any residual spreading rate-dependent variations in CO_2 outgassing (Berner, 1990a,b; Brady and Gislason, 1997; Staudigel et al., 1989, 1990a,b). Increased CO_2 flux from mantle plumes most likely occurred during the relatively short emplacement times of individual LIPs but the time-integrated effect may not be very important on the million year time scale (Marty and Tolstikhin, 1998), an assessment supported by new proxy measurements of pCO_2 that support models (e.g. Caldeira and Rampino, 1990; Dessert et al., 2001) showing that increases associated with a major LIP emplacement decay away on less than a million year time scale (Schaller et al., 2011).

The generally high pCO_2 levels and warm polar climates that characterized the mid-Cretaceous to early Eocene may have had a substantial contribution from the protracted subduction of Tethyan pelagic carbonates deposited on the Indian plate during northward drift from $\sim$ 120 Ma until the collision of Greater India with Asia (Lhasa block) at $\sim$ 50 Ma (Edmond and Huh, 2003; Hansen et al., 2008; Kent and Muttoni, 2008; Schrag, 2002). The ensuing long-term trend of decreasing pCO_2 levels and temperatures from 50 Ma to the onset of Antarctic glaciation at 34 Ma may thus have resulted from re-equilibration to the reduced CO_2 flux with the shutdown of the Tethyan decarbonation factory. Concomitantly, intense weathering of the Deccan Traps as they drifted into the equatorial humid belt may have increased the consumption of CO_2 (Dessert et al., 2003; Kent and Muttoni, 2008).

In this paper, we elaborate on the tectonic forcing of pCO_2 variations using plate tectonic reconstructions in a paleolatitudinal reference frame and attempt to quantify (a) the decarbonation potential of Tethyan subduction since $\sim$ 120 Ma as a potential additional source of CO_2, and (b) the silicate weathering potential for higher consumption of CO_2 of continental areas and especially highly weatherable basaltic provinces as they drifted through the equatorial humid belt, the most potent venue for continental silicate weathering (Dessert et al., 2003). We evaluate the relative contributions of these modes of steering atmospheric pCO_2 as well as other alternative mechanisms, including proposed changes

in organic carbon burial inferred from trends in $\delta^{13}C$ carbonate records (Katz et al., 2005) and the Himalayan uplift-weathering hypothesis (Raymo and Ruddiman, 1992; Raymo et al., 1988). The degree of sensitivity of global climate to changes in atmospheric pCO_2 is difficult to gauge but we mainly seek to explain the pattern of generally high pCO_2 levels from the CTM to EECO ($\sim$ 90 to 50 Ma) and the decrease to generally low pCO_2 levels that characterize the Oligocene to present (from $\sim$ 34 Ma). Modeling studies point to threshold decreases in atmospheric pCO_2 as the most likely causes for widespread Antarctic glaciation at around the Eocene–Oligocene boundary (Oi-1, $\sim$ 34 Ma; DeConto and Pollard, 2003; DeConto et al., 2008) and the onset of permanent Northern Hemisphere glaciations in the late Pliocene ($\sim$ 3 Ma; Lunt et al., 2008).

The main outcome of our calculations is that they point to the viability and primacy of variations in carbon sinks rather than sources, especially changes in silicate weathering consumption as continents in general and those land masses with basaltic provinces in particular drifted through climate belts, on controlling atmospheric pCO_2 over at least the past 120 Ma.

"... there is a special need, in both carbon cycle and climate modeling, to consider only those land areas that have sufficient rain and are sufficiently warm to exhibit appreciable chemical weathering." (R. A. Berner and Z. Kothalava, 2001)

2 Paleogeographic reconstructions from 120 Ma to present

In the absence of compelling evidence for long-term secular changes in global ocean floor production rates, we assume that the background CO_2 outgassing rate held steady and was comparable to the present-day global volcanic CO_2 emission rate from spreading centers, mantle plumes and arc volcanoes with a preferred estimate of $\sim$ 260 Mt CO_2 yr^{-1} or 5.91×10^{12} mol CO_2 yr^{-1}, with a range of plausible estimates of 180 to 440 Mt CO_2 yr^{-1} (Gerlach, 2011; Marty and Tolstikhin, 1998). To estimate contributions of CO_2 outgassing from the subduction of carbonate-rich sediments and consumption of CO_2 from silicate weathering of continental areas as they drifted through different climate zones, we generated paleogeographic reconstructions of the main continents using a composite apparent polar wander path (APWP) (Fig. 2; Table 1) and the finite rotation poles used by Besse and Courtillot (2002) from Muller and Roest (1992), Muller et al. (1993) and Srivastava and Tapscott (1986). The composite APWP uses paleopoles from all the main continents rotated to common coordinates (in this case, North America) and averaged in a sliding 20 Myr window every 10 Myr. The mean paleopole for 60 to 120 Ma is an average of global igneous data from Kent and Irving (2010) for a standstill in APW in North American coordinates; we averaged their 60,

Table 1. APW paths used for paleogeographic reconstructions.

A1 (Ma)	A2 (Ma)	N	A95 (°)	NAM		SAM		AFR		EUR		IND		AUS		ANT	
				Lat (° N)	Lon (° E)	Lat (° N)	Lon (° E)	Lat (° N)	Lon (° E)	Lat (° N)	Lon (° E)	Lat (° N)	Lon (° E)	Lat (° N)	Lon (° E)	Lat (° N)	Lon (° E)
10	8.3	54	2.0	85.0	168.1	85.9	151.0	85.3	173.5	85.4	162.5	86.2	216.4	87.0	254.3	86.0	160.8
20	18.9	38	2.7	83.3	164.2	84.7	133.8	83.9	175.9	84.0	154.8	84.0	246.8	82.8	287.8	85.4	151.9
30	29.5	23	3.8	81.5	169.2	83.7	132.6	81.8	190.7	82.8	158.1	79.1	266.1	76.6	291.0	85.1	162.2
40	40.0	24	3.2	79.5	174.4	82.6	139.2	79.0	201.1	81.3	162.4	73.1	272.4	71.7	289.8	84.3	172.4
50	52.2	31	3.4	77.9	179.3	82.1	141.8	76.9	210.3	80.9	164.4	63.3	276.4	68.2	293.0	84.7	174.7
60*	*	4	1.7	75.9	192.8	82.4	162.8	74.4	221.9	80.7	184.0	52.5	277.1	65.1	292.9	84.6	203.5
70*	*	4	1.7	75.9	192.8	83.2	157.7	74.2	224.4	81.0	182.5	39.1	280.0	64.4	298.5	86.6	209.5
80*	*	4	1.7	75.9	192.8	83.3	163.5	71.7	231.3	81.0	180.9	31.6	282.1	62.5	302.0	87.6	243.4
90*	*	4	1.7	75.9	192.8	84.8	161.1	68.2	239.5	80.8	179.7	24.2	288.2	61.3	309.3	88.5	341.6
100*	*	4	1.7	75.9	192.8	86.0	178.1	63.5	247.4	80.8	178.5	16.3	293.6	59.3	316.1	85.5	11.7
110*	*	4	1.7	75.9	192.8	87.9	217.6	59.8	254.9	80.6	178.9	11.3	294.9	57.2	325.2	80.5	22.0
120*	*	4	1.7	75.9	192.8	86.9	284.3	56.3	262.0	80.4	180.5	6.2	298.4	54.3	335.0	74.5	26.8

Paleopoles from different continents (NAM, North America; SAM, South America; AFR, Africa; EUR, Eurasia; IND, India; AUS, Australia; ANT, East Antarctica) had been transferred to common (NAM) coordinates using rotation parameters from Besse and Courtillot (2002) and averaged in 20 Myr windows stepped every 10 Myr. The mean paleopoles of the composite APW path were then transferred from NAM coordinates to the different continents. Mean paleopoles for 10 to 50 Ma are from Besse and Courtillot (2003); mean paleopole for 60–120 Ma is the standstill superpole in NAM coordinates from Kent and Irving (2010). A1 is age of center of 20 Myr averaging window, A2 is mean age of poles in the 20 Myr window, N = number of paleomagnetic pole entries, Lat is latitude and Lon is longitude of mean paleomagnetic pole and A95 is its radius of circle of 95 % confidence. * Based on average of mean poles listed in Kent and Irving (2010; Table 6) for 60, 80, 100 and 120 Ma windows in NAM coordinates and propagated to other continents via interpolated Euler poles from Besse and Courtillot (2002).

80, 100 and 120 Ma mean poles, which are independent but not significantly different, to derive a 60–120 Ma superpole. Mean paleopoles for 10 to 50 Ma, which are dominated by global igneous data and thus also less prone to be biased by sedimentary inclination error, are from Besse and Courtillot (2002, 2003). The composite APWP should record the geocentric axial dipole field, hence the different APWP for the various continents shown in Fig. 2 simply reflect their relative motions according to the finite rotation model. Uncertainty in latitudinal positions of the continents should be on the order of the radii of circles of 95 % confidence around the mean paleopoles (∼ 3°; Table 1).

The main elements of the plate tectonic scenario are the convergence of Greater India with the Lhasa block, which was accreted to Asia before the Late Jurassic (Allègre et al., 1984; Chang and Cheng, 1973), and the convergence of Arabia with the Iran block, which was accreted to Asia during the Late Triassic–Early Jurassic Cimmerian orogeny (e.g. Muttoni et al., 2009; Zanchi et al., 2009) and was only moderately disrupted by oblique subduction of the Tethyan Ocean in the Cretaceous (Moghadam et al., 2009). A related tectonic feature is the extrusion of the SE Asian blocks during the indentation of India into Asia (Molnar and Tapponnier, 1975). There is a vast literature on various aspects of the tectonics of the Himalaya and adjacent Tibetan Plateau (e.g. more than 330 cited references in a review paper by Yin and Harrison, 2000 and more than 500 cited references in one by Hatzfeld and Molnar, 2010), but what is critical to our analysis is to locate within these reconstructions the position of the Asian margin (Lhasa, Iran) and of the SE Asian blocks, which was done as follows.
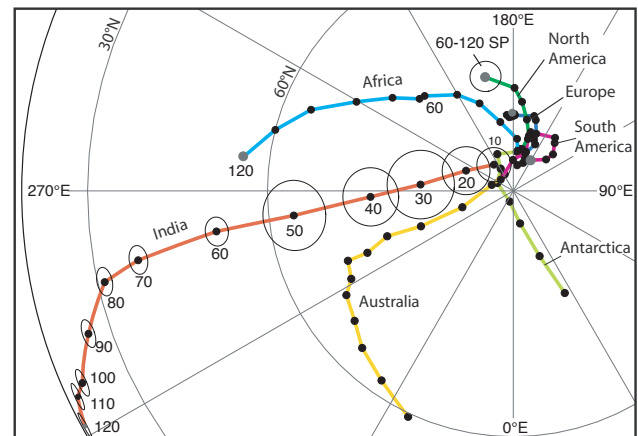

Fig. 2. Apparent polar wander paths for Africa, Antarctica, Australia, Eurasia, India, North America and South America based on a composite APWP using paleopoles from all the main continents that were brought to common coordinates using finite rotation poles used by Besse and Courtillot (2002), averaged with a sliding 20 Myr window every 10 Myr, and the mean poles transferred back to the different continents; hence the differences in APWP for the various continents reflect relative motions according to the finite rotation poles used for the plate reconstructions. Mean paleopoles for 10 to 50 Ma are from Besse and Courtillot (2002, 2003); mean paleopole for 60 to 120 Ma is an average of global igneous data (superpole labeled 60–120 Ma SP with 95 % confidence circle and based on 60, 80, 100 and 120 Ma mean poles from Kent and Irving, 2010) for a standstill in apparent polar wander in North American coordinates (Table 1). Circles of 95 % confidence that are shown on the India APWP are in common for the APWP projected to other continents.

Table 2. Total rotation poles for the SE Asian blocks.

Age	W. Sumatra			N. Indochina			S. Indochina–E. Sumatra–Java			C. Indochina–Borneo		
Ma	Lat	Lon	Ω	Lat	Lon	Ω	Lat	Lon	Ω	Lat	Lon	Ω
0	0.0	0.0	0.0	0.0	0.0	0.0	0.0	0.0	0.0	0.0	0.0	0.0
5	13.7	94.5	5.2	11.5	90.7	5.3	11.5	90.7	5.3	11.5	90.7	5.3
10	11.4	96.2	9.2	9.4	92.0	9.2	9.4	92.0	9.2	9.4	92.0	9.2
15	14.1	102.2	9.7	7.5	91.5	9.7	7.5	91.5	9.7	7.5	91.5	9.7
30	10.6	90.8	21.9	7.2	86.6	22.2	7.2	86.6	22.2	7.2	86.6	22.2
40	4.6	93.3	28.8	5.9	88.6	28.5	1.9	90.2	29.1	4.1	90.4	33.1
50	4.5	93.6	29.3	5.8	89.0	29.0	1.8	90.6	29.6	4.0	90.7	33.6
60	3.4	99.3	30.2	4.6	95.0	29.6	0.7	96.4	30.2	2.8	95.8	34.3
70	3.5	99.0	29.9	4.7	94.5	29.3	0.8	96.0	30.0	2.9	95.4	34.0
80	3.6	98.5	29.8	4.8	94.1	29.3	0.9	95.5	30.0	3.0	95.0	34.0
90	3.6	98.1	30.0	4.9	93.7	29.5	1.0	95.1	30.2	3.1	94.7	34.2
100	3.7	97.7	30.0	4.9	93.3	29.5	1.0	94.7	30.1	3.1	94.3	34.2
110	3.7	97.8	30.2	4.9	93.4	29.7	1.0	94.8	30.4	3.1	94.4	34.3
120	3.6	98.2	30.4	4.8	93.8	29.9	0.9	95.3	30.6	3.0	94.8	34.6

Rotation poles (Lat = latitude ° N, Lon = longitude ° E, Ω = rotation angle, positive counterclockwise) obtained by multiplying the paleomagnetic Euler poles of Eurasia (derived from Table 1) with the step-by-step Euler poles of the SE Asian blocks relative to Siberia (Eurasia) accumulated in the 0–40 Ma time window (derived from Replumaz and Tapponnier, 2003). For the previous 50–120 Ma interval, the SE Asia blocks are considered tectonically coherent and moved with Siberia (Eurasia). N = North, S = South, E = East, W = West, C = Central.

1. The southern (collisional) margin of the Lhasa block was drawn assuming that it coincided with the northern margin of Greater India (which is much easier to place using the APWP described above) at full India–Lhasa collision at 50 Ma; for pre-50 Ma times, the Lhasa margin was kept coherent and therefore rotated with Asia. The ∼ 50 Ma collision age, instrumental to locating the position of the margin, is based on several lines of geological evidence (Garzanti, 2008; Garzanti et al., 1987; Zhu et al., 2005; and references therein), and is supported by the marked decrease in convergence rate between India and Eurasia observed in the Indian Ocean between magnetic Anomaly 22 (∼ 49.5 Ma) and Anomaly 21 (∼ 48.5 Ma) (Copley et al., 2010; Patriat and Achache, 1984; see also Cande and Stegman, 2011; Molnar and Stock, 2009). An age of ∼ 50 Ma for the India–Lhasa collision is preferred to the much younger age of ∼ 35 Ma envisaged by Aitchison et al. (2007) and Ali and Aitchison (2008) essentially for the arguments made by Garzanti (2008). Our reconstructions are in substantial agreement with the available albeit sparse paleomagnetic data indicating that the margin had a paleolatitude comprised between ∼ 10° N and ∼ 20° N in the Cretaceous–early Cenozoic (Achache et al., 1984; Chen et al., 1993, 2012). Other results and compilations of paleomagnetic data that try to take into account sedimentary flattening of paleomagnetic directions suggest that collision of northern India with the Lhasa block occurred at 46 ± 8 Ma (Dupont-Nivet et al., 2010) and that the southern margin of the Lhasa block extended as far

south as 20° N during the Eocene (Lippert et al., 2011), which we regard as in substantial agreement with our reconstructed tectonic framework given the uncertainties in reference paleopoles.

2. Following similar reasoning, the southern (collisional) margin of the Iran block was drawn assuming that it coincided with the northern margin of Arabia at full collision at ∼ 20 Ma. The Arabia–Iran collision may have started at ∼ 35 Ma based on geologic evidence (Agard et al., 2005; Allen and Armstrong, 2008); however, complete western Tethys closure seems not to have occurred until ∼ 20 Ma based on recent apatite fission-track data indicating that the last oceanic lithosphere between Arabia and Eurasia was not consumed until the early Miocene (Okay et al., 2010).

3. The position of the SE Asian blocks (north, central, and south Indochina, west and east Sumatra, Borneo, and Java) have been reconstructed in the 0–40 Ma interval using the (cumulative) rotation poles of Replumaz and Tapponnier (2003) relative to Siberia (Eurasia) (Table 2). For the previous 50–120 Ma interval, the SE Asian blocks are considered tectonically coherent and moved with Siberia (Eurasia). Accordingly, our Cretaceous reconstructions are similar to those of Chen et al. (1993) with Indochina placed using Cretaceous paleomagnetic data from Yang and Besse (1993) across paleolatitudes spanning from ∼ 10° N to 30° N close to Siberia. Moreover, our 65 Ma reconstruction predicts a paleolatitude for western Yunnan (North Indochina

block) that is consistent, within paleomagnetic resolution, with a paleolatitude of $17° ± 9°$ N calculated for the area from (sparse) paleomagnetic data from the Paleocene (Yang et al., 2001). Southward extrusion of the SE Asian blocks basically stopped at about 15 Ma with cessation of seafloor spreading in the South China Sea (Briais et al., 1993) even though overall southerly movement continued as Eurasia rotated clockwise according to its APWP. Our reconstructions are similar to the classic India–SE Asia indentor-extrusion model (Molnar and Tapponnier, 1975; Replumaz and Tapponnier, 2003; Royden et al., 2008) and differ from alternative reconstructions that question evidence for extrusion and locate the SE Asian blocks since before the onset of India–Asia collision at essentially the latitudes they are found today (Aitchison et al., 2007; Hall et al., 2008; see also exchange between Garzanti, 2008 and Aitchison et al., 2008). Hall et al. (2008) support their fixist reconstructions citing paleomagnetic data from Borneo and surrounding regions (Fuller et al., 1999; Schmidtke et al., 1990) that (a) do not seem to indicate a clear pattern of clockwise rotations, and (b) show no consistent southward displacement of blocks over the Cenozoic, both expected from the extrusion model. As acknowledged by Fuller et al. (1999), however, the quality of the paleomagnetic data from Borneo is problematical given that many results come from igneous intrusions with no control on paleo-horizontal and "the intimate mixing throughout Borneo of rotated and unrotated results is easier to explain in terms of remagnetization than by a special distribution of local shears". The details of the paleolatitudinal evolution of Borneo can hardly be resolved by these data. However, results from the Late Cretaceous and early Cenozoic Segamat basalts and supporting data from the Kuantan dike swarm all from the Malaysia Peninsula indicate paleolatitudes at time of emplacement of $20°$ N (compared to a present-day latitude of $\sim 2.5°$ N) (Richter et al., 1999) and provide in our opinion robust (e.g. not influenced by sedimentary inclination flattening) paleomagnetic data in support of the SE Asia southward extrusion model and Eurasia clockwise rotation.

To summarize in a broader paleogeographic context, Greater India resided for much of the Mesozoic in the southern hemisphere as part of the classical Gondwana supercontinental assembly (Smith and Hallam, 1970), which began to disperse in the Late Jurassic with the opening of the Somali basin (Rabinowitz et al., 1983) and the separation of East Gondwana (which included India, Madagascar, Antarctica, and Australia) from West Gondwana (Africa and South America). Greater India commenced its ~ 6000 km northward drift toward Lhasa (Asia) when it separated (with Madagascar) from Antarctica at around 120 Ma (Fig. 3a) and continued its journey after separation from Madagascar at

around 84 Ma, approached the equatorial belt ($5°$ S–$5°$ N) at 65 Ma (Fig. 3b) and began to collide with Lhasa (Asia) at around 50 Ma (Fig. 3c). The extrusion of the SE Asian blocks with the indentation of India into Asia was such that at ~ 30 Ma Borneo was approaching the equatorial humid belt (Fig. 3d). Convergence between Arabia–Iran caused final collision at ~ 20 Ma, whereas the southward extrusion of SE Asia largely ceased by ~ 15 Ma (Fig. 3e). Continued clockwise rotation of Eurasia gradually brought SE Asia to its present position during which time New Guinea, on the northern margin of the Australia plate, impinged on the equatorial humid belt from the south (Fig. 3f).

3 Did the Tethyan CO_2 factory produce Cretaceous–Eocene greenhouse climate?

The northward drift of India involved the subduction under Asia of oceanic crust that must have transited through the equatorial belt (Fig. 3a–c). This is because the paleomagnetic (i.e. latitudinal) constraints indicate that the Lhasa (Asia) southern margin remained in the northern hemisphere ($10°$ N–$20°$ N) from practically the time India separated from Antarctica at ~ 120 Ma until incipient collision at ~ 50 Ma. In modern oceans, equatorial regions are generally associated with upwelling and high organic productivity, giving rise to enhanced deposition of biogenic sediments (Berger and Winterer, 1974) that sequester CO_2 from the atmosphere. This has been especially true since the diversification of planktonic marine protists by the mid-Mesozoic, when open oceans became important loci of carbonate deposition, progressively replacing shallow water carbonates (Wilkinson and Walker, 1989). Calcareous nannoplankton became the most efficient sediment-forming group in Cretaceous oceans, sometimes forming thick chalk deposits, whereas planktonic foraminifers became relevant sediment-producers only since the Late Cretaceous (Erba, 2004). Biogenic sediments deposited on oceanic crust are more readily subducted than shallow water carbonates on buoyant continental crust, hence pelagic sediments are more prone to metamorphic decarbonation, potentially augmenting the global flux of CO_2 to the atmosphere (Caldeira, 1992; Volk, 1989). The subduction of Tethyan sea floor from 120 to 50 Ma may thus have constituted a productive source of additional CO_2, which according to some scenarios may have been responsible for the generally equable climates in the Cretaceous to Eocene (Edmond and Huh, 2003; Hansen et al., 2008; Kent and Muttoni, 2008; Schrag, 2002). Alternatively, much of the subducted carbon may have remained buried in a deep-seated mantle reservoir (Selverstone and Gutzler, 1993). Here we attempt to estimate the maximum amount of subducted carbon as a source of CO_2 to the atmosphere by invoking high biogenic productivity on oceanic crust and assuming that an appreciable fraction of the subducted carbon is returned to the atmosphere.
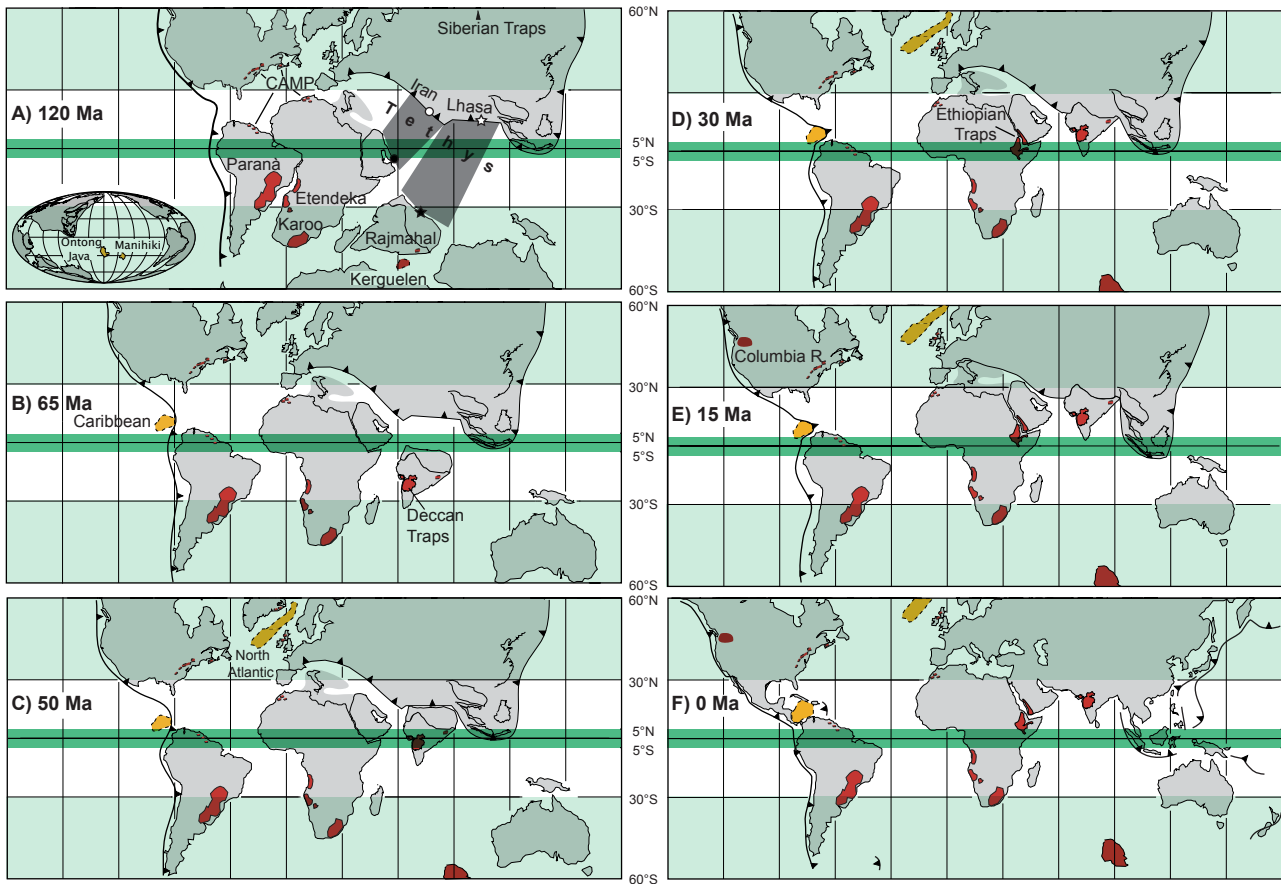
Fig. 3. Paleogeographic reconstructions based on a composite APWP (Table 1, Fig. 2), the finite rotation poles given by Besse and Cour-
tillot (2002) from Muller and Roest (1992), Muller et al. (1993), and Srivastava and Tapscott (1986) for the major continents and the rotation
poles of Replumaz and Tapponnier (2003) for SE Asian blocks, as discussed in text. **(A)** 120 Ma at about Magnetic Anomaly M0; **(B)** 65 Ma
at about Anomaly 29; **(C)** 50 Ma at about Anomaly 21; **(D)** 30 Ma at about Anomaly 11; **(E)** 15 Ma at about Anomaly 5B; **(F)** present-day
geography. The equatorial humid belt ($P > E$: precipitation > evaporation) between 5° S and 5° N is represented by darker green shading,
the temperate humid belts ($P > E$) from 30° to beyond the latitudinal limits (60°) of our paleogeographic reconstructions are represented
by lighter green shading, with the intervening arid belts ($P < E$) unshaded, all based on general circulation climate model with idealized
geography by Manabe and Bryan (1985). Large continental basaltic provinces are shown in red, large submarine provinces in orange. Paleo-
geographic maps were made with PaleoMac software (Cogné, 2003).

We estimated the productivity of the Tethyan CO_2 factory
over the Cretaceous–Cenozoic by reconstructing the latitudi-
nal component of motion for a point on the northern margin
of the Indian plate (filled star in Fig. 3a) compared with the
latitudinal evolution of a point on the Lhasa southern margin
(unfilled star in Fig. 3a). The paleolatitude curves (Fig. 4a)
were used to predict the timing of subduction of oceanic crust
attached to Greater India that was loaded with equatorial
(5° S–5° N) bulge sediments. In a simple 2-plate model, the
onset of northward motion of Greater India at ∼ 120 Ma pre-
saged the onset of subduction of the equatorial bulge under-
neath the Lhasa margin at around 97 Ma and until the bulge
that formed under the equatorial belt at around 72 Ma was
subducted at ∼ 55 Ma and the last sediments were consumed
in the trench at 50 Ma. In other words, a full equatorial load

of sediment was probably continuously subducted in south-
ern Asia trenches from at least ∼ 97 Ma to collision at 50 Ma.

The amount of equatorial bulge sediments subducted with
time can be estimated from the loading time, loading area,
and mass accumulation rate, as follows:

1. The time spent by the Tethyan crust under the pre-
   sumed 5° S–5° N upwelling belt (loading time) was cal-
   culated acknowledging that the Tethyan crust was load-
   ing sediments under the 5° S–5° N belt since well be-
   fore the onset of India–Asia convergence; we therefore
   assumed an initial, nominal loading duration of 20 Myr
   to which we added the loading times directly derived
   from the plate's latitudinal velocity (Fig. 4b). For exam-
   ple, oceanic crust entering the Lhasa trench at ∼ 80 Ma
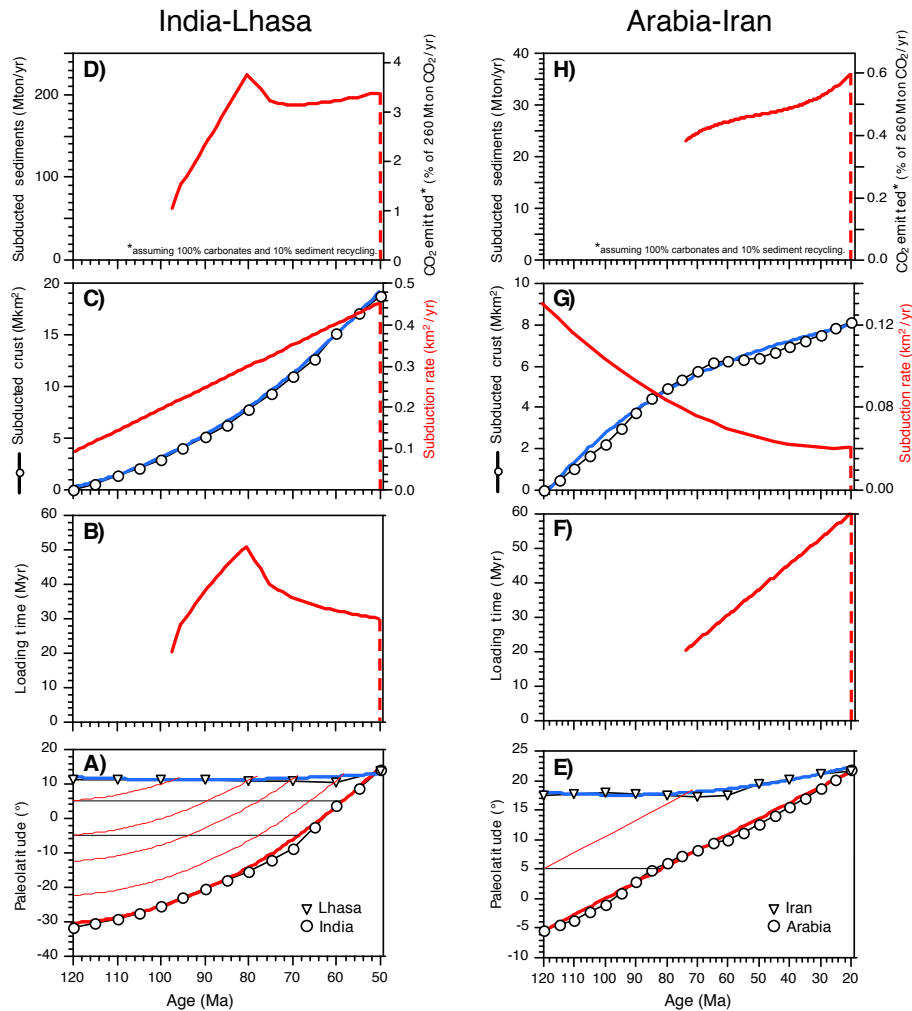   (Fig. 4a) was already sediment-loaded for 20 Myr when

Fig. 4. Estimates of decarbonation in Tethyan subduction factory. Panels **(A)**–**(D)** refer to the subduction of Tethyan crust between Greater India and Lhasa (Asia). **(A)** Paleolatitude curves for northern Greater India (filled star in Fig. 3a) and southern Lhasa block (unfilled star in Fig. 3a) with 2nd order polynomial fits used to calculate the subduction time and the loading time of oceanic crust during passage through hypothesized equatorial upwelling belt (5° S–5° N). **(B)** Sediment loading time for passage through equatorial upwelling belt (5° S–5° N) of oceanic crust subducted under Asia. Curve starts at 97 Ma with a nominal 20 Myr loading time because the oceanic crust was sitting in the equatorial belt since appearance of pelagic carbonates and well before onset of subduction. **(C)** Amount of Tethyan crust as function of time between northern Greater India and southern Lhasa block that was eventually subducted under Asia plotted with a 2nd order polynomial fit resampled every 1 Myr (blue line) and red curve showing subduction rate (scale on right) as 1st derivative of the polynomial subduction curve. **(D)** Amount of equatorial bulge sediments on Tethyan crust subducted under Asia per unit time as a function of geologic age. The axis on the right is the CO_2 emitted by these sediments expressed as percentage of the present-day global volcanic CO_2 emission rate of 260 Mt yr^{-1}, assuming the sediments were 100 % carbonates and 10 % recycled. Panels **(E)**–**(H)** refer to the subduction of Tethyan crust between Arabia and Iran (Asia) following the same procedure illustrated for India–Lhasa in panels **(A)**–**(D)**, with the only notable differences that the time scale extends to 20 Ma and the paleolatitude curves – in **(E)** – are for the southeastern margin of Arabia (filled circle in Fig. 3a) and the western margin of the Iran block (unfilled circle in Fig. 3a).

it started moving from 5° S at 120 Ma across the equatorial belt to 5° N at 89 Ma thus accumulating additional ∼ 31 Myr of loading (total of ∼ 51 Myr at subduction; Fig. 4b). As another example, oceanic crust entering the Lhasa trench at ∼ 70 Ma (Fig. 4a) was already sediment-laden for 20 Myr when it crossed the equatorial belt from ∼ 93 Ma to ∼ 78 Ma accumulating

an additional ∼ 16 Myr of loading (total of ∼ 36 Myr at subduction; Fig. 4b).

2. The surface area of Indian oceanic crust displaced northward at any given time and eventually consumed at the trench (subduction rate) was calculated from the paleogeographic reconstructions (Fig. 3 and additional ones) and found to steadily increase

from $\sim 0.09\,\mathrm{km}^2\,\mathrm{yr}^{-1}$ to $\sim 0.45\,\mathrm{km}^2\,\mathrm{yr}^{-1}$ for a total subducted crust of $\sim 19.0\,\mathrm{Mkm}^2$ (Fig. 4c). Most of this crust ($\sim 14.7\,\mathrm{Mkm}^2$) resided on or crossed the equatorial upwelling belt before being subducted, whereas the remainder ($\sim 4.3\,\mathrm{Mkm}^2$) was located between $5°\,\mathrm{N}$ and the Lhasa margin and presumably never got loaded with equatorial sediments (see Fig. 3a).

3. A nominal mass accumulation rate (MAR) of $1.5\,\mathrm{g\,cm}^{-2}\,\mathrm{kyr}^{-1}$ ($15\,\mathrm{t\,km}^{-2}\,\mathrm{yr}^{-1}$) for the Tethyan equatorial belt $5°\,\mathrm{S}$–$5°\,\mathrm{N}$ was derived from estimates for the Cretaceous equatorial Pacific Ocean (Ogg et al., 1992), which is within the range of values found for the Cenozoic equatorial Pacific (Mitchell and Lyle, 2005; Mitchell et al., 2003).

Summarizing and clarifying the above, oceanic crust transiting under the equatorial upwelling belt gets a full biogenic (calcareous and biosiliceous) sediment load that is estimated by multiplying the loading time (1) by the loading area (2) by the MAR value (3). This subducted load is found to vary between $\sim 60\,\mathrm{Mt\,yr}^{-1}$ at $\sim 120\,\mathrm{Ma}$ up to $\sim 220\,\mathrm{Mt\,yr}^{-1}$ at $\sim 80\,\mathrm{Ma}$ and dropping to virtually zero at $50\,\mathrm{Ma}$ (Fig. 4d). Even allowing the subducted sediment to be entirely carbonate, a recycling rate of $10\,\%$ (although generally less) based on $^{10}\mathrm{Be}$ data in arc volcanics (Tera et al., 1986) would imply that the amount of CO_2 that was potentially generated by the decarbonation of Tethyan pelagic biogenic sediments was maximally $\sim 9.7\,\mathrm{Mt\,CO_2\,yr}^{-1}$ at around $80\,\mathrm{Ma}$, corresponding to only $\sim 4\,\%$ of the present-day global volcanic CO_2 emission rate of $\sim 260\,\mathrm{Mt\,CO_2\,yr}^{-1}$ (Fig. 4d).

A similar scenario of convergence and equatorial bulge subduction can be traced between Arabia and Iran in the western Tethys (Fig. 4e–h). Using the procedure outlined above for India, the mean latitudinal velocity of a point on the northeastern margin of Arabia (filled circle in Fig. 3a) is used in conjunction with the paleolatitude evolution of a point on the southwestern Iran margin (unfilled circle in Fig. 3a) to predict that the oceanic crust loaded with equatorial bulge sediments started subducting at around $74\,\mathrm{Ma}$ and ended at $\sim 20\,\mathrm{Ma}$ with the terminal Arabia–Iran collision (Fig. 4e). The loading time of this subducted oceanic crust was estimated to steadily increase from an initial value of $\sim 20\,\mathrm{Myr}$ (for similar reasons previously illustrated for India) to a maximum of $\sim 60\,\mathrm{Myr}$ (Fig. 4f). The subduction rate was found to decrease from $\sim 0.18\,\mathrm{km}^2\,\mathrm{yr}^{-1}$ to $\sim 0.04\,\mathrm{km}^2\,\mathrm{yr}^{-1}$ for a total subducted crust of $\sim 8.1\,\mathrm{Mkm}^2$ (Fig. 4g). Of this crust, only $\sim 2.1\,\mathrm{Mkm}^2$ resided on or crossed the equatorial upwelling belt before being subducted, whereas the remainder presumably never got loaded with equatorial sediments (see Fig. 3a). These numbers lead us to calculate a subducted sediment load that varies between $\sim 23\,\mathrm{Mt\,yr}^{-1}$ at $70\,\mathrm{Ma}$ and $\sim 35\,\mathrm{Mt\,yr}^{-1}$ at $20\,\mathrm{Ma}$ (Fig. 4h); assuming again that the subducted sediments were entirely carbonates and a recycling rate of $\sim 10\,\%$, the maximum amount of CO_2 that was

potentially generated by the decarbonation of these biogenic sediments was $\sim 1.6\,\mathrm{Mt\,CO_2\,yr}^{-1}$ at around $20\,\mathrm{Ma}$, corresponding to only $\sim 0.6\,\%$ of the present-day global volcanic CO_2 emission rate of $\sim 260\,\mathrm{Mt\,CO_2\,yr}^{-1}$ (Fig. 4h).

It appears that subduction decarbonation of Tethyan pelagic sediments may have reached $\sim 10\,\mathrm{MtCO_2\,yr}^{-1}$ from 80 to $50\,\mathrm{Ma}$, which is only $\sim 4\,\%$ of the present-day global volcanic CO_2 emission rate of $260\,\mathrm{Mt\,CO_2\,yr}^{-1}$.

We can also approach this from the long-term mean ocean production rate of $3.4\,\mathrm{km}^2\,\mathrm{yr}^{-1}$ from Rowley (2002), which would imply that $340\,\mathrm{Mkm}^2$ of oceanic crust was subducted globally in the $100\,\mathrm{Myr}$ from $120\,\mathrm{Ma}$ (about when pelagic carbonates and chalks become important) to $20\,\mathrm{Ma}$ (end of major Tethyan subduction after which there has been only minor overall subduction of pelagic carbonates elsewhere, mainly Central America), or nearly 13-fold what was calculated for subduction just of Tethyan crust ($\sim 27\,\mathrm{Mkm}^2$ for India plus Arabia). However, a substantial fraction of the oceanic crust that was subducted must have been in the Pacific which did not systematically transit through the equatorial upwelling belt and consequently probably had a much lower MAR, perhaps by an order of magnitude ($\sim 1.5\,\mathrm{t\,km}^{-2}\,\mathrm{yr}^{-1}$) than for equatorial bulge pelagic sedimentation (Mitchell and Lyle, 2005). Even if additional subduction decarbonation doubled the rate estimated just for Tethyan pelagic sediments, to perhaps $20\,\mathrm{Mt\,CO_2\,yr}^{-1}$, this would nevertheless still be a small fraction (less than $10\,\%$) of the present-day global volcanic CO_2 emission rate. This leads us to conclude that unless its efficiency was much higher (Johnston et al., 2011) the decarbonation subduction factory was a rather modest contributing factor in producing higher pCO_2 and presumably related warm climate in the Cretaceous–Eocene. We also note that the total deep (mantle) carbon storage of about $1000\,\mathrm{Tt\,CO_2}$ for the past $125\,\mathrm{Myr}$ suggested by Selverstone and Gutzler (1993) to be in response to the Alpine–Himalaya collision amounts to about the same magnitude flux ($8\,\mathrm{Mt\,CO_2\,yr}^{-1}$) as the decarbonation flux albeit of opposite sign and would thus further reduce its relative importance as a net long-term source of CO_2. More generally, subduction decarbonation would seem to be precluded as a major source of CO_2 prior to when open oceans became important loci of carbonate deposition with the abundant appearance of calcareous plankton at $\sim 120\,\mathrm{Ma}$. Edmond and Huh (2003) reached similar conclusions about the general efficacy of subduction decarbonation as a source of CO_2.

Mantle CO_2 that emanated from the emplacement of submarine LIPs (e.g. Ontong Java Plateau, Caribbean Plateau) probably significantly increased global pCO_2 levels that may have triggered environmental responses like oceanic anoxic events (e.g. Jenkyns, 2003; Tejada et al., 2009) but for not over much longer durations than each of their relatively short emplacement times (Self et al., 2005). This is because model calculations (Dupré et al., 2003; Misumi et al., 2009) and available supporting proxy measurements (Schaller et al.,

2011) indicate that the excess CO_2 would be adsorbed by negative feedback mechanisms on less than a million year time scale. In fact, continental LIPs are likely to be net CO_2 sinks due to enhanced consumption from their weathering (Dessert et al., 2003; Schaller et al., 2012).

4   Variable weathering sinks of CO_2

If the long-term source flux of CO_2 stayed basically constant and experienced only transient changes, persistent variations in CO_2 sink fluxes must have been in the driver's seat in controlling the concentration of atmospheric pCO_2. The most important CO_2 sink is weathering of continental silicates (Walker et al., 1981), a negative feedback mechanism dependent on surface temperature and runoff as a function of the CO_2 greenhouse effect and incorporated in most quantitative carbon-cycling models (e.g. Berner, 1991, 1994, 2006; Berner and Kothalava, 2001; Berner et al., 1983; Goddéris and Joachimski, 2004; Goddéris et al., 2008).

Recent evaluations have emphasized the importance of continental basalt weathering as a major sink for atmospheric CO_2, representing anywhere from one-third to nearly one-half of the CO_2 consumption flux from weathering of all continental silicates even though subaerial basalt provinces today constitute less than 5 % of world land area (Table 2 in Dessert et al., 2003). The compilation of Dessert et al. (2003) also shows that for a given gross basin lithology (granitic or basaltic), chemical weathering and CO_2 consumption rates are strongly dependent on runoff and temperature, which are markedly potent in the equatorial humid belt. It is noteworthy that SE Asia in the equatorial humid belt with a mean annual temperature of 25 °C and nearly 140 cm yr^{-1} runoff has by far the highest CO_2 consumption flux (1.033×10^{12} mol yr^{-1} = 45.5 Mt CO_2 yr^{-1}), which constitutes about 25 % of the total CO_2 consumption flux estimated for all basaltic provinces and small volcanic islands (4.08×10^{12} mol yr^{-1} = 180 Mt CO_2 yr^{-1} for total land area of 7.249 Mkm^2; Dessert et al., 2003), even though SE Asia represents less than 8 % of their combined surface area. In contrast, basalt provinces in cold or dry regions are not weathering rapidly and are thus consuming far less CO_2. For example, the Siberian Traps, a LIP that was emplaced in the latest Permian and presently straddles the Arctic Circle with a mean annual temperature of -10 °C and 40 cm yr^{-1} runoff, contributes a paltry 1.3 % (2.3 Mt CO_2 yr^{-1}) to the overall basalt CO_2 consumption flux even though it represents about 11 % of the surface area of all continental basalt provinces and small volcanic islands today (Dessert et al., 2003). The Ethiopian Traps, with a comparable surface area to the Siberian Traps, are just within the tropical arid belt with a much higher mean annual temperature of 21 °C but only 13 cm yr^{-1} runoff and hence end up contributing ~ 3 % (5.3 Mt CO_2 yr^{-1}) to the overall basalt total CO_2 consumption flux (Dessert et al., 2003). Mg and Ca-poor granitic
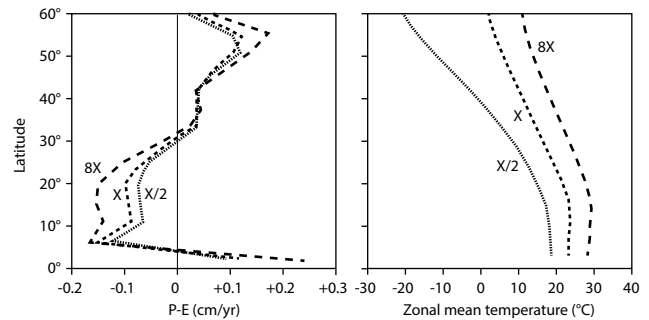

Fig. 5. Latitudinal distributions of (left panel) zonal average precipitation minus evaporation ($P - E$) and (right panel) zonal mean surface air temperature based on a general circulation model with an annual mean insolation and idealized geography obtained for various multiples of atmospheric pCO_2 (pre-industrial) values, shown here ranging from one-half ($X/2$) to eight fold ($8X$) (extracted from Figs. 4 and 19 in Manabe and Bryan, 1985).

terranes have total CO_2 consumption fluxes that are 2 to 10 times lower than basaltic provinces in comparable climate conditions (Dessert et al., 2001; Gaillardet et al., 1999).

To gauge the latitudinal position of climate belts in the past, we use values for zonal mean annual surface air temperature and the difference between precipitation and evaporation ($P - E$) based on a general circulation model from Manabe and Bryan (1985) with idealized geography, an annual mean insolation, and atmospheric pCO_2 concentrations that vary from one-half to 8-times the modern (pre-industrial: 280 ppm) value (Fig. 5). Compared with studies of silicate weathering rate using more comprehensive global climate numerical models (e.g. Donnadieu et al., 2006; Godderis et al., 2008) that include a variety of feedbacks as well as monsoons and other phenomena related to details of geography, the idealized zonal model employed here has the advantage, at this stage, of allowing us to keep the latitudinal dependency of climate more or less fixed while the distribution of land masses varies with plate tectonics. Indeed, their idealized zonal climate model "... completely bypasses the interaction of climate and the carbon cycle itself" (Manabe and Bryan, 1985, p. 11705).

Although the amplitude or climate severity of $P - E$ increases with increasing pCO_2, the latitudinal positions of the crossovers ($P - E = 0$) stay relatively fixed (Manabe and Bryan, 1985) (Fig. 5, left panel). Accordingly, we set the equatorial humid belt ($P > E$) as occurring between 5° S and 5° N and the hemispheric limits of the tropical arid belts ($P < E$) as extending from 5° to 30° latitude and that of the temperate humid belts from 30° to the latitudinal limits (60°) of our paleogeographic maps (Fig. 3). Zonal mean temperatures generally increase with higher pCO_2 but for any given pCO_2 level they are uniformly high in the tropics (nominally 23° S to 23° N) before decreasing to about two-thirds of equatorial values by the lower latitude regions of

the temperate humid belts (30° N or S) and to around freezing (0 °C) by 60° N or S for today's $p\mathrm{CO_2}$ level (Fig. 5, right panel). The most potent and persistent combination of high temperature and high moisture for silicate weathering clearly resides in the equatorial humid belt (5° S–5° N, constituting 44 Mkm^2 or 8.7 % of Earth's total surface area) at any $p\mathrm{CO_2}$ level and that is where we focus attention in estimating $\mathrm{CO_2}$ consumption rates.

5   Quantification of $\mathrm{CO_2}$ silicate weathering sinks

Total continental area in the equatorial humid belt was relatively steady at ~ 12 Mkm^2, which is a little more than one-quarter (27 %) of the available surface area in this zone and about 8 % of present total continental land area (~ 150 Mkm^2), from at least 120 Ma to around 65 Ma (Fig. 6a; see also paleogeography in Fig. 3a and b). Over this time interval, South America had a decreasing areal contribution that was essentially balanced by Africa plus Arabia's increasing areal contribution in the equatorial humid belt. Other land areas had almost negligible contributions until the arrival of Greater India, whose northward passage through the equatorial humid belt provides the distinctive humped signature of the total area curve (Fig. 6a). From the peak of 15 Mkm^2 at ~ 55 Ma, total land area within the equatorial humid belt decreased with the northward indentation of India into Asia and leveled out at around 11 Mkm^2 by 25 Ma when the southerly motion of SE Asia (plus the widening equatorial expanse of South America and the northerly motion of New Guinea attached to Australia) balanced the decreasing contributions from the narrowing equatorial expanse of Africa.

The only large land-based basalt province straddling the equatorial humid belt during the entire Mesozoic was the 201 Ma (earliest Jurassic) Central Atlantic magmatic province (CAMP; Marzoli et al., 1999), whereas the 250 Ma Siberian Traps remained in high ($> 60°$ N) latitudes, the 130 Ma Parana and Entendeka provinces of South America and Africa were in the austral tropical arid belt, and the ~ 120 Ma Rajmajal Traps formed poleward of 50° S in the austral temperate humid belt (Fig. 3). CAMP basalts were apparently thin (100–200 m-thick) but emplaced over a large area across tropical Pangea (5–10 Mkm^2; Marzoli et al., 1999; McHone 2003), and only minor exposures of lavas in isolated rift basins and widely scattered presumed feeder dikes now remain (McHone, 2003). The bulk of the CAMP lavas were probably weathered, eroded or buried soon after their emplacement, very likely within a few hundred thousand years of volcanic activity as suggested by estimates of atmospheric $p\mathrm{CO_2}$ from paleosols interbedded and overlying CAMP lavas in eastern North America (Schaller et al., 2012) and tantalizing indications of rapid global cooling (Schoene et al., 2010). In any case, we suppose that any remaining exposed CAMP fragments were probably too small or had
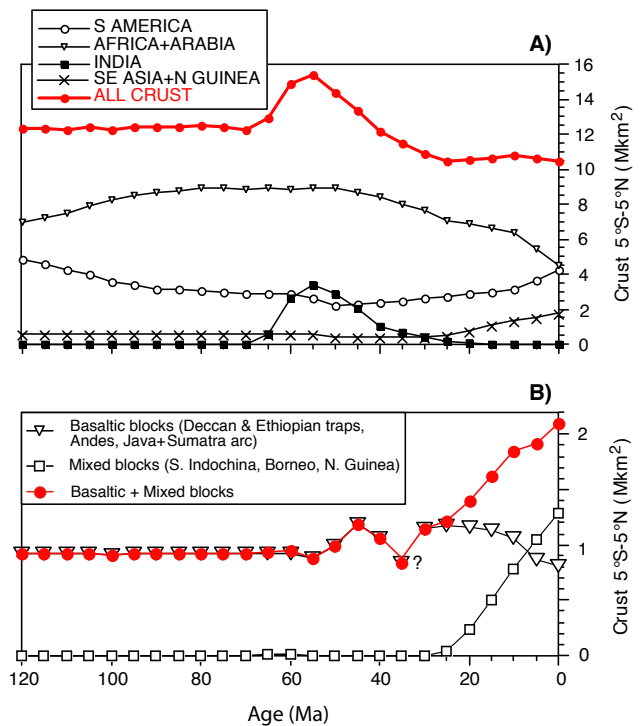

Fig. 6. (A) Estimates of land area within equatorial humid belt (5° S–5° N) as a function of time since 120 Ma obtained by applying the composite APWP (Table 1; Fig. 2) and finite rotation poles of Besse and Courtillot (2002) for major continental blocks and the rotation poles of Replumaz and Tapponnier (2003) for SE Asian blocks as discussed in text. **(B)** Estimates of key (most weatherable in the most favorable environment) land areas comprised of volcanic arc provinces (Java, Sumatra, Andes), large basaltic provinces (Deccan Traps, Ethiopian Traps), and mixed igneous-metamorphic provinces (South Indochina, Borneo, New Guinea) in the equatorial humid belt (5° S–5° N) as a function of time from 120 Ma to present. The rest of the world's continental regions in the equatorial humid belt are generally characterized by low elevation (Amazon and Congo basins), hence weathering tends to be low and transport-limited.

already drifted out of the equatorial humid belt to be important factors in weathering $\mathrm{CO_2}$ consumption by Cretaceous times. The more or less constant area (0.9 Mkm^2) of basaltic rocks from 120 to 50 Ma is mostly in the Andes with some contribution from the Sumatra–Java arc (Fig. 6b).

The Deccan Traps (current surface area of 0.5 Mkm^2; original volume of ~ 2 Mkm^3; Courtillot and Renne, 2003) were emplaced at ~ 65 Ma in the austral arid belt (Fig. 3b) and in our view became a major consumer in the long-term $\mathrm{CO_2}$ budget only when the Indian plate with the Deccan drifted into the equatorial humid belt at 50 Ma (Fig. 3c), just about when Greater India began to collide with Asia. At 30 Ma, the Ethiopian Traps (current surface area of 0.4 Mkm$^2 = 1/2$ of original extent; Rochette et al., 1998) erupted virtually on the equator just as the Deccan Traps drifted out of the

equatorial humid belt where Java and Sumatra already began to impinge (Fig. 3d). Tectonic extrusion of SE Asia may have effectively ceased by 15 Ma but a gradual southerly drift due to Eurasia clockwise rotation brought Borneo into the equatorial humid belt (Fig. 3e) where it was eventually joined by New Guinea (attached to Australia) coming from the south (Fig. 3f). Today, there are more than $2\,\mathrm{Mkm}^2$ of highly weatherable basaltic and mixed arc and related rocks in the equatorial humid belt (Fig. 6b).

To estimate the total CO_2 consumption rate of the varying land areas within the equatorial humid belt as a function of time, we use the following rates for the dominant lithologies. The rate for basaltic-rich provinces (Deccan and Ethiopian Traps, Andes, Java and Sumatra arc) was set to a nominal value of $100\,\mathrm{t\,CO_2\,yr^{-1}}$ per km^2; this value represents a rounded estimate falling in the lower (conservative) side of a present-day total CO_2 consumption span ranging from $84.5\,\mathrm{t\,CO_2\,yr^{-1}}$ per km^2 $(1.92 \times 10^6\,\mathrm{mol\,CO_2\,yr^{-1}\,km^{-2}})$ for SE Asia in toto to $282\,\mathrm{t\,CO_2\,yr^{-1}}$ per km^2 $(6.41 \times 10^6\,\mathrm{mol\,CO_2\,yr^{-1}\,km^{-2}})$ for the island of Java alone (Dessert et al., 2003). A nominal $1/2$ of the basalt weathering rate $(50\,\mathrm{t\,yr^{-1}}$ per $\mathrm{km}^2)$ was applied to mixed (basaltic-granitic-gneissic) land areas (South Indochina, Borneo, New Guinea) following Dessert et al. (2001); for example, the basaltic island of Réunion ($21°$ S; $\sim 240\,\mathrm{cm\,yr^{-1}}$ runoff, $19\,°\mathrm{C}$ mean annual temperature) has an annual total CO_2 consumption rate that is roughly twice that of the climatically similar, mixed basaltic-granitic island of Puerto Rico ($18°$ N, $\sim 360\,\mathrm{cm\,yr^{-1}}$ runoff, $22\,°\mathrm{C}$ mean annual temperature; Fig. 2 in Dessert et al., 2001). Total CO_2 consumption rates for continental cratonic regions are expected to be much lower due to much less weatherable granitic lithologies and generally low topographic relief (i.e. transport-limited regimes; see Sect. 7 below). With all due caveats, we use $5\,\mathrm{t\,yr^{-1}}$ per km^2 for continental cratonic areas, a rate that is an order of magnitude less than for mixed lithology land areas like New Guinea and compatible with the relative sense of total CO_2 consumption rates deduced from the chemistry of large rivers in such areas (Gaillardet et al., 1999).

In applying these weathering rates to the past, we would note that paleotemperature estimates from planktonic foraminiferal oxygen isotope records point to tropical climate throughout the Eocene only a few degrees warmer than modern sea-surface temperatures (Pearson et al., 2007). Extrapolation to the past of modern total CO_2 consumption rates for the tropics should therefore provide reasonably compatible estimates as far as the temperature component is concerned although the ancient weathering rates are likely to be underestimated due to more vigorous hydrological cycles when atmospheric $p\mathrm{CO}_2$ levels were higher (Manabe and Bryan, 1985; Held and Soden, 2006), as they almost invariably were over the past 120 Myr and longer.

Total CO_2 consumption values corresponding to these rates were calculated for areas of subaerial basalts and mixed
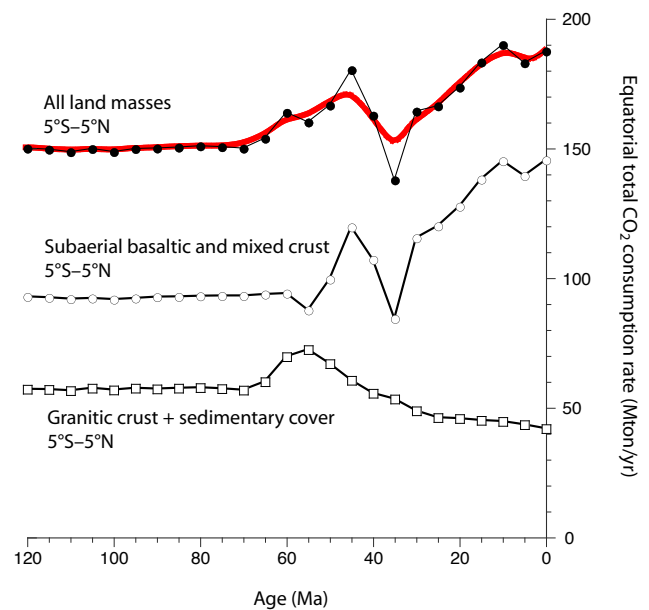

Fig. 7. Total CO_2 consumption rates from silicate weathering since 120 Ma of land areas in equatorial humid belt ($5°$ S–$5°$ N) obtained by multiplying a nominal CO_2 consumption rate of $100\,\mathrm{t\,CO_2\,yr^{-1}\,km^{-2}}$ for basaltic provinces and $50\,\mathrm{t\,yr^{-1}\,km^{-2}}$ for mixed basaltic-metamorphic provinces (Dessert et al., 2003) and an order of magnitude less ($5\,\mathrm{t\,yr^{-1}\,km^{-2}}$) for the remaining continental land areas (Gaillardet et al., 1999) to the corresponding cumulative distribution curves in Fig. 6. Note that these total consumption rates should be divided by 2 for net CO_2 consumption rates because half of the CO_2 consumed by silicate weathering is returned to the atmosphere–ocean during carbonate precipitation. For example, total CO_2 consumption of $190\,\mathrm{Mt\,CO_2\,yr^{-1}}$ would correspond to a net CO_2 consumption of $190/2 = 95\,\mathrm{Mt\,CO_2\,yr^{-1}}$, or $\sim 35\,\%$ of present-day global volcanic CO_2 outgassing of $260\,\mathrm{Mt\,CO_2\,yr^{-1}}$. For reference, the consumption of $1\,\mathrm{Mt\,CO_2\,yr^{-1}}$ can be sustained by introducing into the equatorial humid belt or rejuvenating roughly $10\,000\,\mathrm{km}^2$ (or $\sim 20\,000\,\mathrm{km}^2$ for net) of the SE Asia arc terrane every million years.

crust and for the remaining continental cratonic areas in the equatorial humid belt in 5 Myr intervals (Fig. 7). Under these assumptions, areas of subaerial basalts and mixed crust contribute about 50 % more than the remaining much vaster continental cratonic areas (all in the equatorial humid belt) from 120 to 50 Ma, after which the contribution of subaerial basalts and mixed crust eventually increases to nearly 3.5 times that of the remaining continental cratonic areas. The combined CO_2 consumption profile for all subaerial crust in the equatorial humid belt (top curve in Fig. 7) has much of the character of the potent subaerial basalts and mixed crust component, for example, the downward blip at ~ 35 Ma is essentially due to an apparent gap of highly weatherable basalts in the equatorial humid belt between the northward drift of the Deccan Traps out of the belt before the eruption of the Ethiopian Traps at 30 Ma (Fig. 6b). We

cannot exclude that this short-term variation might in part be an artifact associated with uncertainties of a few degrees in continent paleolatitudes combined with the tight and fixed latitudinal bounds of the equatorial humid belt in the simple zonal climate model we used. Hence the smoothed curve in Fig. 7 may provide at this juncture a more substantiated representation of the secular change in total equatorial consumption of CO_2. Even allowing that the total consumption flux of CO_2 should be halved to account for the CO_2 returned to the atmosphere–ocean during carbonate precipitation, it is remarkable that the net CO_2 consumption rate of up to $190/2 = 95\,\mathrm{Mt}\,CO_2\,\mathrm{yr}^{-1}$ from silicate weathering of only a small fraction of total land with basaltic and mixed crust provinces currently residing in the equatorial humid belt may balance a substantial fraction ($\sim 35\,\%$) of the present-day global volcanic emission rate of $260\,\mathrm{Mt}\,CO_2\,\mathrm{yr}^{-1}$.

6 Himalayan uplift-erosion hypothesis

According to the uplift-erosion hypothesis (Raymo and Ruddiman, 1992), uplift of the Himalayas and Tibetan Plateau as a consequence of the India–Asia collision resulted in enhanced silicate weathering rates and higher associated consumption of CO_2, causing Earth's climate to cool with the eventual formation of Antarctic ice sheets by ~ 34 Ma. This was largely based on the supposition that the progressive increase in $^{87}Sr/^{86}Sr$ values of marine carbonates since ~ 40 Ma (Hess et al., 1986; Richter et al., 1992) was due to enhanced delivery of radiogenic Sr from increased global chemical weathering rates from mountain building, especially the uplift of the Himalayas (Raymo et al., 1988). It is not clear in this model what would have been responsible for initiating decreasing atmospheric pCO$_2$ over the prior 10 Myr since the $^{87}Sr/^{86}Sr$ seawater curve is essentially flat from at least 50 Ma (when cooling starts according to $\delta^{18}O$ data, see Fig. 1a) to 40 Ma. More importantly, others have argued rather persuasively that most of the overall increase in $^{87}Sr/^{86}Sr$ resulted from the unroofing and chemical erosion of particularly radiogenic Himalayan rocks, such as leucogranites (Edmond, 1992) and metasediments (Harris, 1995) including metamorphosed limestones (Quade et al., 1997), in which case the $^{87}Sr/^{86}Sr$ seawater curve would not serve as a simple proxy for *global* weathering rates of continental silicates.

The general principle of the uplift-erosion hypothesis is nevertheless difficult to dismiss and the drift-weathering idea proposed here bears a general resemblance to it: both call upon tectonic mechanisms (uplift, plate motion) to initiate and sustain higher CO_2 consumption via silicate weathering. Compared to a carbon cycling model driven on the supply-side, a sink-side model like the uplift-erosion hypothesis may have to contend with the absence of an effective feedback mechanism that is well-coupled to the climate system to stabilize atmospheric pCO$_2$ levels even over relatively

short geologic time scales (e.g. Berner and Caldiera, 1997; Broecker and Sanyal, 1998). Kump and Arthur (1997) modified the Himalayan uplift-erosion concept by invoking compensatory factors to high local (Himalayan) chemical erosion and associated CO_2 drawdown: according to their model, global chemical erosion rates did not increase over the Cenozoic because higher erosion rates in the Himalayan region were more or less balanced by decreased erosion rates elsewhere as climate cooled. What caused CO_2 to decline, according to them, was that the continents somehow became more susceptible to chemical erosion, or more weatherable, since the Miocene (20 Ma), even though their calculated weatherability factor was flat or even decreased from 50 to 20 Ma over which time global cooling started, atmospheric pCO$_2$ levels declined and there was even a major glacioeustatic fall at 34 Ma (Fig. 1).

But what if tectonic uplift occurred closer to the equator: global climate would cool with the drawdown of CO_2 but the resulting decreased silicate weathering and reduced CO_2 consumption elsewhere might not be able to compensate for the continued drawdown of CO_2 due to the presence of more weatherable landmasses in the relatively warm and wet conditions of the equatorial humid belt. This is effectively the drift-weathering scenario and may be the ongoing case today with the high landmasses of the SE Asian islands like Java, Sumatra, Borneo (world's 3rd largest island at $0.75\,\mathrm{Mkm}^2$ with mountain peaks rising to over 4000 m), as well as New Guinea (2nd largest island after Greenland at $0.79\,\mathrm{Mkm}^2$ with peaks rising to nearly 5000 m) impinging upon the equatorial humid belt and shedding prodigious amounts of sediment intensely weathering in the heat and humidity of the lowland aprons, even though atmospheric pCO$_2$ levels are very low (probably as a result). This is also reflected by the global annual fluvial sediment flux from the world's main drainage basins to the oceans that shows a disproportionately high contribution to the global sediment yield by the SE Asian islands straddling the modern equator (Milliman, 1990).

Although the weathering flux per unit area on the Ganges floodplain may be appreciable (West et al., 2002), it seems to us that the specific Himalayan uplift-erosion hypothesis does not actually do enough early enough and for long enough in terms of CO_2 drawdown from silicate weathering to account for the cooling over the Cenozoic that led to the formation of major polar ice sheets. Besides, there are mountains in many parts of the world that at any given time are being actively eroded. The action really needs to happen in the equatorial humid belt where whenever significant weatherable lithologies are inserted via horizontal plate motion and/or vertical uplift – as is presently happening – negative feedbacks may not be efficient enough to inhibit net CO_2 drawdown and an eventual ice age.

7 Transport-limited negative feedback

The relatively small surficial carbon reservoir compared to the large carbon fluxes implies that there is close parity on million year time scales between inputs (volcanic outgassing and metamorphism) and outputs (silicate weathering followed by deposition of carbonate minerals and burial of organic carbon) to maintain a stable level of CO_2 in the atmosphere (Berner and Caldeira, 1997). This fine balance requires a negative feedback that depends strongly on the level of atmospheric CO_2. A powerful concept for policing the CO_2 content of the atmosphere is the CO_2-silicate weathering feedback mechanism of Walker et al. (1981) that underlies the BLAG model (Berner et al., 1983) and the GEOCARB lineage of supply-side carbon cycling models (Berner, 2004): increases or decreases in CO_2 outgassing induce an opposing response from higher or lower chemical weathering rates via associated greenhouse effects. A stabilizing negative feedback is more difficult to identify in a sink-side model, for example, an uplift-weathering mechanism (i.e. model of Raymo and Ruddiman, 1992) left uncoupled to the CO_2 content of the atmosphere would eventually produce a crash in atmospheric pCO_2 (Kump and Arthur, 1997). After evaluating alternative mechanisms, such as a possible albeit tenuous link between erosion and organic carbon burial (Raymo, 1994), Broecker and Sanyal (1998) concluded that the pCO_2 level of the atmosphere almost certainly has to act as the controller of a silicate weathering feedback.

So what is to keep atmospheric pCO_2 from plunging or wildly oscillating in our drift-weathering, sink-side model? We suggest that as a continental silicate province drifts into the equatorial humid belt and is subject to relatively intense chemical weathering, there may eventually be a transition from weathering-limited to transport-limited regimes with thickening of cation-deficient soils that will tend to retard further chemical weathering of the bedrock; this is likely to characterize cratonic areas with low relief (Kump et al., 2000; West et al., 2005). In the case of continental basaltic provinces entering the equatorial humid belt, they are provided with initial relief from plume head uplift and the stacking of lava flows that would prolong the weathering-limited phase; nevertheless, they may eventually be either consumed by intense weathering or drift out of the intense weathering regime, resulting in a reduction to their contribution to CO_2 drawdown. The Deccan and Ethiopian Traps soon enough drifted out of the equatorial humid belt and escaped this fate of complete consumption by weathering and erosion, whereas most of the once widespread CAMP lavas were evidently largely consumed probably not long after their emplacement at around 201 Ma (Schaller et al., 2012), leaving only a few remnants amongst the now-dispersed Atlantic-bordering continents.

An interesting exception is SE Asia, a major CO_2 sink (Dessert et al., 2003) that has been straddling the equatorial humid belt since at least 25 Ma and which, as a set of island arc terranes, has been continuously rejuvenated by uplift and magmatism and therefore subjected to persistent intense weathering. There would be rather weak negative feedbacks in this case, making SE Asia (along with New Guinea) a prime candidate responsible for very weakly regulated consumption of enough CO_2 to plunge Earth's climate system into a glacial mode and keep it there in the later part of the Cenozoic. Higher east–west sea-surface temperature gradients and more vigorous Walker circulation in the equatorial Pacific, much like normal conditions today, apparently resulted from the end of continual El Nino due to global shoaling of the oceanic thermocline at around 3 Ma (Fedorov et al., 2006; Ravelo, 2006); we are tempted to speculate that increased rainfall over the SE Asia–New Guinea equatorial archipelago may have caused sufficiently higher CO_2 consumption from runoff-enhanced silicate weathering to trigger Northern Hemisphere glaciations.

8 Temperate-latitude safety valves

Although significant variations in potential sources of CO_2 such as oceanic crust production rates and hydrothermal activity cannot be precluded even though they are notoriously difficult to calibrate, the drift-weathering model of varying CO_2 sinks arising from the changing latitudinal distribution of land masses, and especially basaltic provinces and island arc terranes, provides a measurable and hence testable mechanism to account for long-term variations in atmospheric pCO_2 levels over the Late Cretaceous and Cenozoic, and further back in Earth's history.

The key is the sporadic presence of highly weatherable continental basalt provinces in the equatorial humid belt, the engine of Earth's climate system that is characterized by warm temperatures and high rainfall at widely varying atmospheric pCO_2 levels. With no highly weatherable basaltic provinces in the equatorial humid belt from at least 120 to 50 Ma, atmospheric pCO_2 levels tended to be elevated giving rise to warm climates such as the intervals centered on the CTM and the EECO. These super-greenhouse conditions would have activated enhanced weathering of continents and especially basaltic provinces in a warmer and wetter temperate humid belt. For example, many of the lavas of the British Tertiary igneous province, a subprovince of the North Atlantic igneous province LIP of late Paleocene to early Eocene age that was emplaced and remained at mid-paleolatitudes of ∼45° N (Ganerød et al., 2010), were erupted subaerially (Saunders et al., 1997) and are often closely associated with well-developed laterites, such as the 30 m-thick unit belonging to the Interbasaltic Formation in Antrim, Northern Ireland (Hill et al., 2000) and the red boles on the Isles of Mull and Skye in Scotland (Emeleus et al., 1996). Elsewhere in ostensibly temperate Europe, bauxite was named from Les Baux-de-Provence in France (∼44° N) for a lateritic aluminum ore that mainly formed on carbonate rocks
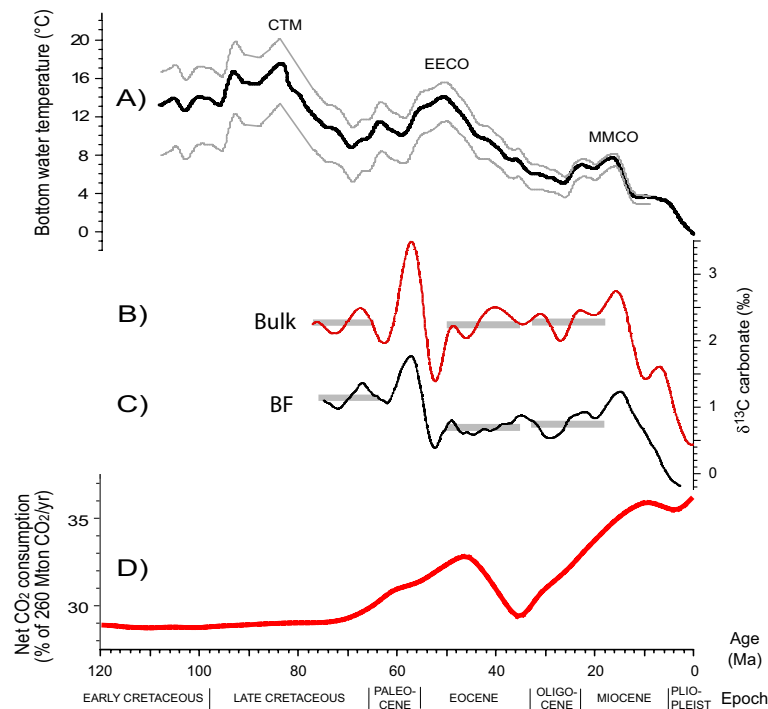
Fig. 8. (A) Bottom water temperatures (Cramer et al., 2011; see caption to Fig. 1 for explanation); **(B)** δ^{13}C carbonate data from whole sediment (Bulk) (smoothed SSA curve from Katz et al., 2005) and **(C)** δ^{13}C carbonate data from benthic foraminifera (BF) from the Pacific (smoothed trend from Cramer et al., 2009), with mean values over selected intervals (77–65, 50–35, 33–18 Ma) shown by gray bars in both curves; **(D)** Secular change in net (one-half of total) CO_2 consumption rate from silicate weathering of all land masses in equatorial humid belt (5° S–5° N) (smoothed curve from Fig. 7) expressed as percentage of the present-day global volcanic CO_2 emission rate of 260 Mt CO_2 yr^{-1} (Gerlach, 2011; Marty and Tolstikhin, 1998).

of Jurassic and Cretaceous age (Retallack, 2010). In western North America, some of the highest calculated denudation rates for crystalline bedrock for non-glacial times were documented in the Green River Basin (42° N) and ascribed to enhanced silicate dissolution rates associated with elevated atmospheric pCO$_2$ levels that occurred during the EECO (Smith et al., 2008).

These and other examples support the concept that basaltic provinces outside the equatorial humid belt effectively act as safety valves that limit extreme accumulations of CO_2 in the atmosphere. Equable climates are the norm or default mode; ice ages are the exception, due to fortuitous latitudinal distributions of potent silicate weathering sinks of CO_2 with only weak negative feedbacks. In other words, the silicate-weathering thermostat, so effective at the high temperature end, sometimes cannot sufficiently decrease weathering rates of highly weatherable (i.e. basaltic) continental provinces in the equatorial humid belt that is only loosely coupled to atmospheric pCO$_2$ levels, thus paving the way to an ice age as in the late Cenozoic (or at the extreme, a Snowball Earth: Hoffman and Schrag, 2002; Godderis et al., 2003).

9 Role of organic carbon burial

Excess burial of organic carbon has been suggested as contributing to the progression from greenhouse climate of the Mesozoic to icehouse conditions that prevailed by the late Cenozoic (Katz et al., 2005) and is briefly considered here. The relative fractions of carbonate and organic carbon buried in sediments are reflected in carbon isotopes of carbonate produced in surface waters (Broecker and Woodruff, 1992; Kump, 1991) as revealed, for example, by the bulk sediment record compiled by Katz et al. (2005) that mainly reflects calcareous plankton. A comparison between this (δ^{13}C$_{carb}$) dataset and the benthic foraminifera δ^{13}C$_{BF}$ record compiled by Cramer et al. (2009), which is reasonably continuous from ~77 Ma to present (Fig. 8), also provides insight into the evolving role of the biological pump that transfers carbon from the shallow to deep water reservoirs (Volk and Hoffert, 1985).

The organic fraction (f_{org}) of the total carbon burial flux at steady state can be estimated according to Kump and Arthur (1999):

$$f_{org} = \left(\delta'_w - \delta_{carb}\right)/\Delta_B$$

where δ'_w is the average carbon isotopic composition of the riverine flux (assumed to be $-5\,‰$), δ_{carb} is the isotopic composition of carbonate sediments that reflect the oceanic carbon reservoir, and Δ_B represents the isotopic difference between organic matter and carbonate deposited from the ocean. If Δ_B is assumed to be constant (say $-29\,‰$) from 77 to 15 Ma, the mean δ_{carb} of $2.3\,‰$ would imply a typical average f_{org} of 0.25; a dependence of Δ_B on ambient pCO$_2$ (Kump and Arthur, 1999) would tend to slightly increase the average organic burial fraction with declining atmospheric pCO$_2$ levels since ~ 35 Ma, for example, f_{org} would be 0.27 for pCO$_2$ of ~ 350 ppm. The large (up to $\sim 2.5\,‰$) decrease in the bulk sediment (and benthic) records from 15 Ma to present (Fig. 8b and c) was interpreted by Shackleton (1987) as due to a decreasing fraction of organic carbon burial although its origin has remained enigmatic (Broecker and Woodruff, 1992). Katz et al. (2005) suggested that about $1.1\,‰$ of the decrease could be accounted for by the rise of C4 photosynthetic pathways with the remaining $\sim 1.4\,‰$ decrease due to weathering (i.e. unburial) of organic-rich shales. Although France–Lanord and Derry (1997) suggested that net burial of organic carbon during Himalayan sedimentation consumed several times more CO$_2$ than weathering of Himalayan silicates in the Neogene, there seems to be little evidence for increasing net organic carbon burial on global scale to account for cooling climate from the middle Miocene climate optimum (MMCO) (Flower and Kennett, 1994; Miller et al., 1987; Wright et al., 1992; You et al., 2009).

The other prominent feature in the bulk (and benthic) sediment carbon isotope record is the $1.5\,‰$ increase starting at around 62.5 Ma that peaks at 57 Ma and followed by a $2\,‰$ decrease to a prominent trough at 52 Ma (Fig. 8b). The run-up to the peak at 57 Ma implies an increasing fraction of organic carbon burial (f_{org} up to 0.3), which may be related to burial of organic-rich sediments, whereas the subsequent large decrease in carbon isotope values (implying f_{org} decreased to ~ 0.22) starting at around 57 Ma may mark the exhumation and oxidation of organic carbon-rich Tethyan marine sediments during the early stages of the India–Asia collision according to Beck et al. (1995), who suggested that this may have increased atmospheric pCO$_2$ sufficiently to have contributed to global warming in the early Cenozoic (albeit somewhat prior to peak warmth at the EECO).

A comparison between the bulk sediment and benthic carbonate δ^{13}C records (Fig. 8b and c) shows that the average value for benthic data between 77 Ma to just before the Cretaceous–Paleogene boundary perturbation at 65 Ma (D'Hondt et al., 1998) is $1.2\,‰$, about $1.1\,‰$ higher than the bulk sediment δ^{13}C mean of $2.3\,‰$. From 50 Ma, just after the Paleocene–Eocene boundary perturbation (Hilting et al., 2008), to 35 Ma, just before Oi-1 at around the Eocene–Oligocene boundary, as well as from 33 Ma, just after Oi-1, to 18 Ma, just before the MMCO, the benthic means are $0.7\,‰$ or about $1.6\,‰$ lighter compared to the corresponding

bulk sediment means of $2.3\,‰$. It would thus appear that the biological pump spun-up soon after EECO (~ 50 Ma), well before the inception of large Antarctic ice sheets and the strengthening of ocean circulation at Oi-1 at around 34 Ma (e.g. Cramer et al., 2009; Kennett, 1977), and stayed relatively constant from 35–50 to 18–33 Ma. A sustained higher input of nutrients, notably phosphates (Schrag et al., 2002), may have resulted from enhanced weathering of continental silicates starting with the arrival of the Deccan in the equatorial humid belt at ~ 50 Ma (marked also by the formation of abundant cherts in the world's oceans; Muttoni and Kent, 2007). This may have spurred biological productivity even though the fraction of organic carbon burial hardly varied in concert.

10 Conclusions

1. Contrary to what has sometimes been assumed including in our earlier work (Kent and Muttoni, 2008), the degree to which decarbonation of pelagic sediments contributes to atmospheric pCO$_2$ is calculated to be rather modest compared to present-day global volcanic outgassing, suggesting that subduction decarbonation was not a decisive factor in the higher atmospheric pCO$_2$ levels associated with warm climates of the Late Cretaceous and early Cenozoic let alone earlier, before proliferation of pelagic carbonate deposition in the deep sea.

2. The small estimated contribution of decarbonation along with the null hypothesis of a constant rate of ocean crust production (Rowley, 2002) suggest that changes in the long-term budget of atmospheric pCO$_2$ are more likely governed by the carbon sinks rather than in response to variations in the carbon supply as typically invoked in many carbon cycling models for at least the late Mesozoic and Cenozoic.

3. To explain long-term changes in atmospheric pCO$_2$, we consider a time-varying CO$_2$ sink model largely driven by the amount of land area, and highly weatherable subaerial basaltic terranes in particular, brought by tectonic plate motions into the equatorial humid belt, the most potent venue for continental silicate weathering and associated consumption of CO$_2$.

4. According to the drift-weathering hypothesis, the long-term decrease in atmospheric pCO$_2$ levels since the EECO was initiated by the arrival of Greater India carrying the highly weatherable Deccan Traps into the equatorial humid belt at around 50 Ma, and was sustained by the emplacement of the 30 Ma Ethiopian Traps near the equator, the southerly tectonic extrusion of SE Asia, an arc terrane that presently is estimated to account for $\sim 1/4$ of the total CO$_2$ consumption by continental basalt weathering and volcanic islands that in

turn represents $\sim 1/3$ of total continental silicate weathering (Dessert et al., 2003), joined by the incursion of New Guinea into the equatorial belt from the south.

5. The equatorial humid belt is likely to maintain potent (warm and wet) conditions for weathering over a broad range of atmospheric $p\text{CO}_2$ levels with only weak negative feedbacks to limit weathering rates, which would therefore tend to dwell on the high side. Low atmospheric $p\text{CO}_2$ levels leading to global cooling and glaciation depend on enhanced and sustained presence of weatherable rocks, especially subaerial basalts, near the equator.

6. Paleosols and other evidence of more intense chemical weathering in temperate latitudes tend to be associated with times of very high atmospheric $p\text{CO}_2$ levels and warm global climates, for example, *terra rossa* between subaerial lavas of the North Atlantic igneous province of late Paleocene to early Eocene age, which evidently acted as safety valves providing the strong negative feedback that acts to squelch a runaway greenhouse when there are insufficient weatherable terranes in the equatorial humid belt to adequately balance CO_2 outgassing.

7. The drift-weathering hypothesis bears some resemblance to the Himalayan uplift-erosion hypothesis of Raymo and Ruddiman (1992) to the extent that it does not seem to make much difference whether more weatherable lithologies are introduced by horizontal plate motion – as we suggest – or as vertical uplift in mountain building processes, as long as it happens close to the warm and humid equatorial belt.

8. Basalt terranes are highly weatherable and thus very effective in CO_2 consumption within the equatorial humid belt but large changes in area of more typical continental lithologies are also capable of affecting the atmospheric $p\text{CO}_2$ balance (Godderis et al., 2003, 2008).

9. Comparison of bulk (mainly planktic) carbonate and benthic carbon isotope records indicates that the biological pump (surface to deep ocean isotopic gradient) increased just after the EECO ($\sim 50\,\text{Ma}$) and continued at more or less the same high level through most of the rest of the Cenozoic, a pattern that could reflect higher productivity associated with increased availability of nutrients from the same silicate weathering in the equatorial humid belt that was drawing down atmospheric $p\text{CO}_2$.

10. The drift-weathering hypothesis provides motivation for obtaining accurate estimates of the latitudinal distribution of landmasses and especially basaltic provinces over time, independent of inferences about sea-floor production rates, and incorporating climate models that

Appendix A

Acronyms and abbreviations.

APWP	apparent polar wander path
CAMP	Central Atlantic Magmatic Province
CTM	Cretaceous Thermal Maximum
EECO	Early Eocene climatic optimum
kyr	10^3 yr
Ma	10^6 yr ago
MAR	mass accumulation rate
Mkm^2	10^6 square-kilometers
MMCO	Middle Miocene climatic optimum
Mt	megaton, 10^9 kilograms
Myr	10^6 yr
$P-E$	precipitation minus evaporation
Tton	teraton, 10^{15} kg
SE Asia	Southeast Asia

take into account factors like relief, lithology and vegetation and include the necessary feedbacks and adequate spatiotemporal resolution for a more comprehensive understanding of the carbon cycle and climate change.

References

Achache, J., Courtillot, V., and Zhou, Y. X.: Paleogeographic and tectonic evolution of southern Tibet since middle Cretaceous time: New paleomagnetic data and synthesis, J. Geophys. Res.,89, 10311–10339, 1984.

Agard, P., Omrani, J., Jolivet, L., and Mouthereau, G.: Convergence history across Zagros (Iran): Constraints from collisional and earlier deformation, Int. J. Earth Sci., 94, 401–419, 2005.

Aitchison, J. C., Ali, J. R., and Davis, A. M.: When and where did India and Asia collide?, J. Geophys. Res., 112, B05423, doi:10.1029/2006JB004706, 2007.

Aitchison, J. C., Ali, J. R., and Davis, A. M.: Reply to comment by Eduardo Garzanti on "When and where did India and Asia collide?", J. Geophys. Res., 113, B04412, doi:10.1029/2007JB005431, 2008.

Ali, J. R. and Aitchison, J. C.: Gondwana to Asia: Plate tectonics, paleogeography and the biological connectivity of the Indian sub-continent from the Middle Jurassic through latest Eocene (166–35 Ma), Earth-Sci. Rev., 88, 145–166, 2008.

Allègre, C. J., Courtillot, V., Tapponnier, P., Hirn, A., Mattauer, M., Coulon, C., Jaeger, J. J., Achache, J., Scharer, U., Marcoux, J., Burg, J. P., Girardeau, J., Armijo, R., Gariepy, C., Gopel, C., Tindong, L., Xuchang, X., Chenfa, C., Guangqin, L., Baoyu, L., Jiwen, T., Naiwen, W., Guoming, C., Tonglin, H., Xibin, W., Wanming, D., Huaibin, S., Yougong, C., Ji, Z., Hongrong, Q., Peisheng, B., Songchan, W., Bixiang, W., Yaoxiu, Z., and Xu, R.: Structure and evolution of the Himalaya-Tibet orogenic belt, Nature, 307, 17–22, 1984.

Allen, M. B. and Armstrong, H. A.: Arabia-Eurasia collision and the forcing of mid-Cenozoic global cooling, Palaeogeogr. Palaeocl., 265, 52–58, 2008.

Beck, R. A., Burbank, D. W., Sercombe, W. J., Olson, T. L., and Khan, A. M.: Organic carbon exhumation and global warming during the early Himalayan collision, Geology, 23, 387–390, 1995.

Beerling, D. J. and Royer, D. L.: Convergent Cenozoic CO_2 history, Nat. Geosci., 4, 418–420, 2011.

Berger, W. H. and Winterer, E. L.: Plate stratigraphy and the fluctuating carbonate line, in: Pelagic Sediments: On Land and Under the Sea, Special Publications of the International Association of Sedimentologists, No. 1, edited by: Hsu, K. J. and Jenkins, H. C., Blackwell Scientific Publications, Oxford, 11–48, 1974.

Berner, R. A.: Global CO_2 degassing and the carbon cycle: Comment on "Cretaceous ocean crust at DSDP sites 417 and 418: Carbon uptake from weathering vs. loss by magmatic outgassing", Geochim. Cosmochim. Acta, 54, 2889–2890, 1990a.

Berner, R. A.: Response to criticism of the BLAG model, Geochim. Cosmochim. Acta, 54, 2892–2893, 1990b.

Berner, R. A.: A model for atmospheric CO_2 over Phanerozoic time, Am. J. Sci., 291, 339–376, 1991.

Berner, R. A.: GEOCARB II: A revised model of atmospheric CO_2 over Phanerozoic time, Am. J. Sci., 294, 56–91, 1994.

Berner, R. A.: The Phanerozoic Carbon Cycle, Oxford University Press, Oxford, p. 150, 2004.

Berner, R. A.: GEOCARBSULF: A combined model for Phanerozoic atmospheric O_2 and CO_2, Geochim. Cosmochim. Acta, 70, 5653–5664, 2006.

Berner, R. A. and Caldeira, K.: The need for mass balance and feedback in the geochemical carbon cycle, Geology, 25, 955–956, 1997.

Berner, R. A. and Kothalava, Z.: GEOCARB III: A revised model of atmospheric CO_2 over Phanerozoic time, Am. J. Sci., 301, 182–204, 2001.

Berner, R. A., Lasaga, A. C., and Garrels, R. M.: The carbonate-silicate geochemical cycle and its effect on atmospheric carbon dioxide over the past 100 million years, Am. J. Sci., 283, 641–683, 1983.

Besse, J. and Courtillot, V.: Apparent and true polar wander and the geometry of the geomagnetic field over the last 200 Myr, J. Geophys. Res., 107, 2300, doi:10.1029/2000JB000050, 2002.

Besse, J. and Courtillot, V.: Correction to "Apparent and true polar wander and the geometry of the geomagnetic field over the last 200 Myr": J. Geophys. Res., 108, 2469, doi:10.1029/2003JB002684, 2003.

Brady, P. V. and Gislason, S. R.: Seafloor weathering controls on atmospheric CO_2 and global climate, Geochim. Cosmochim. Acta, 61, 965–973, 1997.

Briais, A., Patriat, P., and Tapponnier, P.: Updated interpretation of magnetic anomalies and seafloor spreading stages in the South China Sea: Implications for the Tertiary tectonics of southeast Asia, J. Geophys. Res., 98, 6299–6328, 1993.

Broecker, W. S. and Sanyal, A.: Does atmospheric CO_2 police the rate of chemical weathering?, Global Biogeochem. Cy., 12, 403–408, 1998.

Broecker, W. S. and Woodruff, F.: Discrepancies in the oceanic carbon isotope record for the last fifteen million years?, Geochim. Cosmochim. Acta, 56, 3259–3264, 1992.

Caldeira, K.: Enhanced Cenozoic chemical weathering and the subduction of pelagic carbonate, Nature, 357, 578–581, 1992.

Caldeira, K. and Rampino, M. R.: Carbon dioxide emissions from Deccan volcanism and a K/T boundary greenhouse effect, Geophys. Res. Lett., 17, 1299–1302, 1990.

Cande, S. C. and Kent, D. V.: Revised calibration of the geomagnetic polarity time scale for the Late Cretaceous and Cenozoic, J. Geophys. Res., 100, 6093–6095, 1995.

Cande, S. C. and Stegman, D. R.: Indian and African plate motions driven by the push force of the Reunion plume head, Nature, 475, 47–52, 2011.

Chang, C.-F. and Cheng, H.-L.: Some tectonic features of the Mt. Jolmo Lungma area, southern Tibet, China, Scientia Sin., 16, 257–265, 1973.

Chen, W., Yang, T., Zhang, S., Yang, Z., Li, H., Wu, H., Zhang, J., Ma, Y., and Cai, F.: Paleomagnetic results from the Early Cretaceous Zenong Group volcanic rocks, Cuoqin, Tibet, and their paleogeographic implications, Gondwana Res., 22, 461–469, 2012.

Chen, Y., Courtillot, V., Cogne, J.-P., Besse, J., Yang, Z., and Enkin, R. J.: The configuration of Asia prior to the collision of India: Cretaceous paleomagnetic constraints, J. Geophys. Res., 98, 21927–21941, 1993.

Cogné, J.-P. and Humler, E.: Temporal variation of oceanic spreading and crustal production rates during the last 180 My, Earth Planet. Sc. Lett., 227, 427–439, 2004.

Cogné, J. P.: PaleoMac: A Macintosh™ application for treating paleomagnetic data and making plate reconstructions: Geochemistry, Geophysics, Geosystems, 4, 1007, doi:10.1029/2001GC000227, 2003.

Cogné, J. P. and Humler, E.: Trends and rhythms in global seafloor generation rate, Geochem. Geophy. Geosy., 7, Q03011, doi:10.1029/2005GC001148, 2006.

Copley, A., Avouac, J.-P., and Royer, J.-Y.: India-Asia collision and the Cenozoic slowdown of the Indian plate: Implications for the forces driving plate motions, J. Geophys. Res., 15, B03410, doi:10.1029/2009JB006634, 2010.

Courtillot, V. E. and Renne, P. R.: On the ages of flood basalt events, Comptes Rendus Geoscience, 335, 113–140, 2003.

Cramer, B. S., Toggweiler, J. R., Wright, J. D., Katz, M. E., and Miller, K. G.: Ocean overturning since the Late Cretaceous: Inferences from a new benthic foraminiferal isotope compilation, Paleoceanography, 24, PA4216, doi:10.1029/2008PA001683,

2009.

Cramer, B. S., Miller, K. G., Toggweiler, J. R., Barrett, P. J., and Wright, J. D.: Late Cretaceous-Neogene trends in deep ocean temperature and continental ice volume: reconciling records of benthic foraminiferal geochemistry (δ^{18}O and Mg/Ca) with sea level history, J. Geophys. Res.-Oceans, 116, C12023, 2011.

D'Hondt, S., Donaghay, P., Zachos, J. C., Luttenberg, D., and Lindinger, M.: Organic carbon fluxes and ecological recovery from the Cretaceous-Tertiary mass extinction, Science, 282, 276–279, 1998.

DeConto, R. M. and Pollard, D.: Rapid Cenozoic glaciation of Antarctica induced by declining atmospheric CO_2, Nature, 421, 245–249, 2003.

DeConto, R. M., Pollard, D., Wilson, P. A., Palike, H., Lear, C. H., and Pagani, M.: Thresholds for Cenozoic bipolar glaciation, Nature, 455, 652–656, 2008.

Dessert, C., Dupré, B., Francois, L. M., Schott, J. J., Gaillardet, J., Chakrapani, G., and Bajpai, S.: Erosion of Deccan Traps determined by river geochemistry: impact on the global climate and the ^{87}Sr/^{86}Sr ratio of seawater, Earth Planet. Sc. Lett., 188, 459–474, 2001.

Dessert, C., Dupré, B., Gaillardet, J., Francois, L., and Allègre, C.: Basalt weathering laws and the impact of basalt weathering on the global carbon cycle, Chem. Geol., 202, 257–273, 2003.

Donnadieu, Y., Goddéris, Y., Pierrehumbert, R., Dromart, G., Fluteau, F., and Jacob, R.: A GEOCLIM simulation of climatic and biogeochemical consequences of Pangea breakup, Geochem. Geophy. Geosy., 7, Q11019, doi:10.1029/2006GC001278, 2006.

Dupont-Nivet, G., Lippert, P. C., Van Hinsbergen, D. J. J., Meijers, M. J. M., and Kapp, P.: Palaeolatitude and age of the Indo–Asia collision: palaeomagnetic constraints, Geophys. J. Int., 182, 1189–1198, 2010.

Dupré, B., Dessert, C., Oliva, P., Goddeìris, Y., Viers, J., François, L., Millot, R., and Gaillardet, J.: Rivers, chemical weathering and Earth's climate, Comptes Rendus Geoscience, 335, 1141–1160, 2003.

Edmond, J. M.: Himalayan tectonics, weathering processes, and the strontium isotope record in marine limestones, Science, 258, 1594–1597, 1992.

Edmond, J. M. and Huh, Y.: Non-steady state carbonate recycling and implications for the evolution of atmospheric pCO$_2$, Earth Planet. Sc. Lett., 216, 125–139, 2003.

Emeleus, C. H., Allwright, E. A., Kerr, A. C., and Williamson, I. T.: Red tuffs in the Palaeocene lava successions of the Inner Hebrides, Scottish J. Geol., 32, 83–89, 1996.

Engebretson, D. C., Kelley, K. P., Cashman, H. J., and Richards, M. A.: 180 million years of subduction, GSA Today, 2, 93–95, 1992.

Erba, E.: Calcareous nannofossils and Mesozoic Oceanic Anoxic Events, Mar. Micropaleontol., 52, 85–106, 2004.

Fedorov, A. V., Dekens, P. S., McCarthy, M., Ravelo, A. C., deMenocal, P. B., Barreiro, M., Pacanowski, R. C., and Philander, S. G.: The Pliocene paradox (Mechanisms for a permanent El Nino), Science, 312, 1485–1499, 2006.

Flower, B. P. and Kennett, J. P.: The middle Miocene climatic transition: East Antarctic ice sheet development, deep ocean circulation and global carbon cycling, Palaeogeogr. Palaeocl., 108, 537–555, 1994.

France-Lanord, C. and Derry, L. A.: Organic carbon burial forcing of the carbon cycle from Himalayan erosion, Nature, 390, 65–67, 1997.

Fuller, M., Ali, J. R., Moss, S. J., Frost, G. M., Richter, B., and Mahfi, A.: Paleomagnetism of Borneo, J. Asian Earth Sci., 17, 3–24, 1999.

Gaillardet, J., Dupré, B., Louvat, P., and Allègre, C. J.: Global silicate weathering and CO_2 consumption rates deduced from the chemistry of large rivers, Chem. Geol., 159, 3–30, 1999.

Ganerød, M., Smethurst, M. A., Torsvik, T. H., Prestvik, T., Rousse, S., McKenna, C., v. Hinsbergen, J. J., and Hendriks, B. W. H.: The North Atlantic Igneous Province reconstructed and its relation to the Plume Generation Zone: the Antrim Lava Group revisited, Geophys. J. Int., 182, 183–202, 2010.

Garzanti, E.: Comment on "When and where did India and Asia collide?" by Jonathan C. Aitchison, Jason R. Ali, and Aileen M. Davis, J. Geophys. Res., 113, B004411, doi:10.1029/2007JB005276, 2008.

Garzanti, E., Baud, A., and Mascle, G.: Sedimentary record of the northward flight of India and its collision with Eurasia (Ladakh Himalaya, India), Geodinam. Acta, 1, 297–312, 1987.

Gerlach, T.: Volcanic versus anthropogenic carbon dioxide, EOS Trans. Am. Geophys. Union, 92, 201–202, 2011.

Goddéris, Y. and Joachimski, M. M.: Global change in the late Devonian: modeling the Frasnian-Famennian short-term carbon isotope isotope excursions, Paleogeogr. Paleocl., 202, 309–329, 2004.

Godderis, Y., Donnadieu, Y., Nedelec, A., Dupré, B., Dessert, C., Grard, A., Ramstein, G., and Francois, L. M.: The Sturtian "snowball" glaciation: fire and ice, Earth Planet. Sc. Lett., 211, 1–12, 2003.

Godderis, Y., Donnadieu, Y., de Vargas, C., Pierrehumbert, R. T., Dromart, G., and van de Schootbrugge, B.: Causal or casual link between the rise of nannoplankton calcification and a tectonically-driven massive decrease in Late Triassic atmospheric CO_2?, Earth Planet. Sc. Lett., 267, 247–255, 2008.

Hall, R., vanHattum, M. W. A., and Spakman, W.: Impact of India–Asia collision on SE Asia: The record in Borneo, Tectonophysics, 451, 366–389, 2008.

Hansen, J., Sato, M., Kharecha, P., Beerling, D., Berner, R., Masson-Delmotte, V., Pagani, M., Raymo, M., Royer, D. L., and Zachos, J. C.: Target atmospheric CO_2: Where should humanity aim?, Open Atmos. Sci. J., 2, 217–231, 2008.

Harris, N.: Significance of weathering Himalayan metasedimentary rocks and leucogranites for the Sr isotope evolution of seawater during the early Miocene, Geology, 23, 795–798, 1995.

Hatzfeld, D. and Molnar, P.: Comparisons of the kinematics and deep structures of the Zagros and Himalaya and of the Iranian and Tibetan plateaus and geodynamic implications, Rev. Geophys., 48, RG2005, doi:10.1029/2009RG000304, 2010.

Held, I. M. and Soden, B. J.: Robust responses of the hydrological cycle to global warming, J. Climate, 19, 5686–5699, 2006.

Hess, J., Bender, M. L., and Schilling, J.-G.: Evolution of the ratio of strontium-87 to strontium-86 in seawater from Cretaceous to Present, Science, 231, 979–984, 1986.

Hill, I. G., Worden, R. H., and Meighan, I. G.: Geochemical evolution of a palaeolaterite: the Interbasaltic Formation, Northern Ireland, Chem. Geol., 166, 65–84, 2000.

Hilting, A. K., Kump, L. R., and Bralower, T. J.: Variations in the oceanic vertical carbon isotope gradient and their implications for the Paleocene–Eocene biological pump, Paleoceaeanography, 23, PA3222, doi:10.1029/2007PA001458, 2008.

Hoffman, P. F. and Schrag, D. P.: The snowball Earth hypothesis: testing the limits of global change, Terra Nova, 14, 129–155, 2002.

Jenkyns, H. C.: Evidence for rapid climate change in the Mesozoic–Palaeogene greenhouse world, Philos. T. Roy. Soc. Lond. A, 361, 1885–1916, 2003.

Johnston, F. K. B., Turchyn, A. V., and Edmonds, M.: Decarbonation efficiency in subduction zones: Implications for warm Cretaceous climates, Earth Planet. Sc. Lett., 303, 143–152, 2011.

Katz, M. E., Wright, J. D., Miller, K. G., Cramer, B. S., Fennel, K., and Falkowski, P. G.: Biological overprint of the geological carbon cycle, Mar. Geol., 217, 323–338, 2005.

Kennett, J. P.: Cenozoic evolution of Antarctic glaciation, the circum-antarctic ocean and their impact on global paleoceanography, J. Geophys. Res., 82, 3843–3860, 1977.

Kent, D. V. and Irving, E.: Influence of inclination error in sedimentary rocks on the Triassic and Jurassic apparent polar wander path for North America and implications for Cordilleran tectonics, J. Geophys. Res., 115, B10103, doi:10.1029/2009JB007205, 2010.

Kent, D. V. and Muttoni, G.: Equatorial convergence of India and early Cenozoic climate trends, P. Natl. Acad. Sci., 105, 16065–16070, 2008.

Kump, L. R.: Interpreting carbon-isotope excursions: Strangelove oceans, Geology, 19, 299–302, 1991.

Kump, L. R. and Arthur, M. A.: Global chemical erosion during the Cenozoic: Weatherability balances the budgets, in: Tectonic Uplift and Climate Change, edited by: Ruddiman, W. F., Plenum Press, New York, 399–426, 1997.

Kump, L. R. and Arthur, M. A.: Interpreting carbon-isotope excursions: carbonates and organic matter, Chem. Geol., 161, 181–198, 1999.

Kump, L. R., Brantley, S. L., and Arthur, M. A.: Chemical weathering, atmospheric CO_2, and climate, Annu. Rev. Earth Planet. Sc., 28, 611–667, 2000.

Lippert, P. C., Zhao, X., Coe, R. S., and Lo, C.-H.: Palaeomagnetism and $^{40}Ar/^{39}Ar$ geochronology of upper Palaeogene volcanic rocks from Central Tibet: implications for the Central Asia inclination anomaly, the palaeolatitude of Tibet and post-50 Ma shortening within Asia, Geophys. J. Int., 184, 131–161, 2011.

Livermore, R., Hillenbrand, C. D., Meredith, M., and Eagles, G.: Drake Passage and Cenozoic climate: An open and shut case?, Geochem. Geophy. Geosy., 8, Q01005, doi:10.1029/2005GC001224, 2007.

Lunt, D. J., Foster, G. L., Haywood, A. M., and Stone, E. J.: Late Pliocene Greenland glaciation controlled by a decline in atmospheric CO_2 levels, Nature, 454, 1102–1105, 2008.

Manabe, S. and Bryan, K.: CO_2-induced change in a coupled ocean-atmosphere model and its paleoclimatic implications, J. Geophys. Res., 90, 11689–11707, 1985.

Marty, B. and Tolstikhin, I. N.: CO_2 fluxes from mid-ocean ridges, arcs and plumes, Chem. Geol., 145, 233–248, 1998.

Marzoli, A., Renne, P. R., Piccirillo, E. M., Ernesto, M., Gellieni, G., and De Min, A.: Extensive 200-million-year-old continental flood basalts of the Central Atlantic Magmatic Province, Science, 284, 616–618, 1999.

McHone, J. G.: Volatile emissions from Central Atlantic Magmatic Province basalts: Mass assumptions and environmental consequences, in: The Central Atlantic Magnatic Province: Insights from Fragments of Pangea, Geophysical Monograph 136, edited by: Hames, W. E., McHone, J. G., Renne, P. R., and Ruppel, C., American Geophysical Union, Washington, DC, 241–254, 2003.

Miller, K. G., Fairbanks, R. G., and Mountain, G. S.: Tertiary oxygen isotope synthesis, sea level history, and continental margin erosion, Paleoceanography, 2, 1–19, 1987.

Miller, K. G., Kominz, M. A., Browning, J. V., Wright, J. D., Mountain, G. S., Katz, M. E., Sugarman, P. J., Cramer, B. S., Christie-Blick, N., and Pekar, S. F.: The Phanerozoic record of global sea-level change, Science, 310, 1293–1298, 2005a.

Miller, K. G., Wright, J. D., and Browning, J. V.: Visions of ice sheets in a greenhouse world, Mar. Geol., 217, 215–231, 2005b.

Milliman, J. D.: Fluvial sediment in coastal seas: flux and fate, Nat. Resour., 26, 12–22, 1990.

Misumi, K., Yamanaka, Y., and Tajika, E.: Numerical simulation of atmospheric and oceanic biogeochemical cycles to an episodic CO_2 release event: Implications for the cause of mid-Cretaceous Ocean Anoxic Event-1a, Earth Planet. Sc. Lett., 286, 316–323, 2009.

Mitchell, N. C. and Lyle, M. W.: Patchy deposits of Cenozoic pelagic sediments in the central Pacific, Geology, 33, 49–52, 2005.

Mitchell, N. C., Lyle, M. W., Knappenberger, M. B., and Liberty, L. M.: Lower Miocene to Present stratigraphy of the equatorial Pacific sediment bulge and carbonate dissolution anomalies, Paleoceanography, 18, 1038, doi:10.1029/2002PA000828, 2003.

Moghadam, H. S., Whitechurch, H., Rahgoshay, M., and Monsef, I.: Significance of Nain-Baft ophiolitic belt (Iran): Short-lived, transtensional Cretaceous back-arc oceanic basins over the Tethyan subduction zone, C. R. Geoscience, 341, 1016–1028, 2009.

Molnar, P. and Stock, J. M.: Slowing of India's convergence with Eurasia since 20 Ma and its implications for Tibetan mantle dynamics, Tectonics, 28, TC3001, doi:10.1029/2008TC002271, 2009.

Molnar, P. and Tapponnier, P.: Cenozoic tectonics of Asia: effects of a continental collision, Science, 189, 419–426, 1975.

Muller, R. D. and Roest, W. R.: Fracture zones in the North Atlantic from combined Geosat and Seasat data, J. Geophys. Res., 97, 3337–3350, 1992.

Muller, R. D., Royer, J. Y., and Lawver, L. A.: Revised plate motions relative to the hotspots from combined Atlantic and Indian Ocean hotspot tracks, Geology, 21, 275–278, 1993.

Muller, R. D., Sdrolias, M., Gaina, C., Steinberger, B., and Heine, C.: Long-term sea-level fluctuations driven by ocean basin dynamics, Science, 319, 1357–1362, 2008.

Muttoni, G. and Kent, D. V.: Widespread formation of cherts during the early Eocene climate optimum, Palaeogeogr. Palaeocl., 253, 348–362, 2007.

Muttoni, G., Mattei, M., Balini, M., Zanchi, A., Gaetani, M., and Berra, F.: The drift history of Iran from the Ordovician to the Triassic, Special Publications, Geol. Soc. London, 312, 7–29, 2009.

Ogg, J. G., Karl, S. M., and Behl, R. J.: Jurassic through Early Cretaceous sedimentation history of the Central Equatorial Pacific and of Sites 800 and 801, Proc. Ocean Drill. Prog., 129, 571–613, 1992.

Okay, A. I., Zattin, M., and Cavazza, W.: Apatite fission-track data for the Miocene Arabia–Eurasia collision, Geology, 38, 35–38, 2010.

Pagani, M., Zachos, J. C., Freeman, K. H., Tipple, B., and Bohaty, S.: Marked decline in atmospheric carbon dioxide concentrations during the Paleogene, Science, 309, 600–603, 2005.

Pagani, M., Huber, M., Liu, Z., Bohaty, S. M., Henderiks, J., Sijp, W., Krishnan, S., and DeConto, R. M.: The role of carbon dioxide during the onset of Antarctic glaciation, Science, 334, 1261–1264, 2011.

Patriat, P. and Achache, J.: India-Eurasia collision chronology has implications for crustal shortening and driving mechanism of plates, Nature, 311, 615–621, 1984.

Pearson, P. N., Ditchfield, P. W., Singano, J., Harcourt-Brown, K. G., Nicholas, C. J., Olsson, R. K., Shackleton, N. J., and Hall, M. A.: Warm tropical sea surface temperatures in the Late Cretaceous and Eocene epochs, Nature, 413, 481–488, 2001.

Pearson, P. N., vanDongen, B. E., Nicholas, C. J., Pancost, R. D., Schouten, S., Singano, J. M., and Wade, B. S.: Stable warm tropical climate through the Eocene Epoch, Geology, 35, 211–214, 2007.

Quade, J., Roe, L., DeCelles, P. G., and Ojha, T. P.: The Late Neogene ^{87}Sr/^{86}Sr record of lowland Himalayan rivers, Science, 276, 1828–1831, 1997.

Rabinowitz, P. D., Coffin, M. F., and Falvey, D.: The separation of Madagascar and Africa, Science, 220, 67–69, 1983.

Ravelo, A. C.: Walker circulation and global warming: Lessons from the geologic past, Oceanography, 19, 114–122, 2006.

Raymo, M. E.: The Himalayas, organic carbon burial, and climate in the Miocene, Paleoceanography, 9, 399–404, 1994.

Raymo, M. E. and Ruddiman, W. F.: Tectonic forcing of late Cenozoic climate, Nature, 359, 117–122, 1992.

Raymo, M. E., Ruddiman, W. F., and Froelich, P. N.: Influence of late Cenozoic mountain building on ocean geochemical cycles, Geology, 16, 649–653, 1988.

Rea, D. K., Zachos, J. C., Owen, R. M., and Gingerich, P. D.: Global change at the Paleocene-Eocene boundary: climatic and evolutionary consequences of tectonic events, Palaeogeogr. Palaeocl., 79, 117–128, 1990.

Replumaz, A. and Tapponnier, P.: Reconstruction of the deformed collision zone between India and Asia by backward motion of lithospheric blocks, J. Geophys. Res., 108, 2285, doi:10.1029/2001JB000661, 2003.

Retallack, G. J.: Lateritization and bauxitization events, Econom. Geol., 105, 655–667, 2010.

Richter, B., Schmidtke, E., Fuller, M., Harbury, N., and Samsudin, P. D.: Paleomagnetism of Peninsular Malaysia, J. Asian Earth Sci., 17, 477–519, 1999.

Richter, F. M., Rowley, D. B., and DePaolo, D. J.: Sr isotope evolution of seawater: the role of tectonics, Earth Planet. Sc. Lett., 109, 11–23, 1992.

Rochette, P., Tamrat, E., Feraud, G., Pik, R., Courtillot, V., Ketefo, E., Coulon, C., Hoffmann, C., Vandamme, D., and Yirgu, G.: Magnetostratigraphy and timing of the Oligocene Ethiopian traps, Earth Planet. Res. Lett., 164, 497–510, 1998.

Rowley, D. B.: Rate of plate creation and destruction: 180 Ma to present, Geol. Soc. Am. Bull., 114, 927–933, 2002.

Rowley, D. B.: Extrapolating Oceanic Age Distributions: Lessons from the Pacific Region, J. Geol., 116, 587–598, 2008.

Royden, L. H., Burchfiel, B. C., and van der Hilst, R. D.: The geological evolution of the Tibetan Plateau, Science, 321, 1054–1058, 2008.

Royer, D. L.:, Fossil soils constrain ancient climate sensitivity, P. Natl. Acad. Sci., 107, 517–518, 2010.

Saunders, A. D., Fitton, J. G., Kerr, A. C., Norry, M. J., and Kent, R. W.: The North Atlantic Igneous Province, in: Large Igneous Provinces: Continental, Oceanic, and Planetary Flood Volcanism, Geophysical Monograph 100, edited by: Mahoney, J. J. and Coffin, M. F., American Geophysical Union, Washington, D.C., 45–93, 1997.

Schaller, M. F., Wright, J. D., and Kent, D. V.: Atmospheric pCO$_2$ perturbations associated with the Central Atlantic Magmatic Province, Science, 331, 1404–1409, 2011.

Schaller, M. F., Wright, J. D., Kent, D. V., and Olsen, P. E.: Rapid emplacement of the Central Atlantic Magmatic Province as a net sink for CO$_2$, Earth Planet. Sc. Lett., 323–324, 27–39, 2012.

Schmidtke, E., Fuller, M., and Haston, R.: Paleomagnetic data from Sarawak, Malaysian Borneo and the Late Mesozoic and Cenozoic tectonics of Sundaland, Tectonics, 9, 123–140, 1990.

Schoene, B., Guex, J., Bartolini, A., Schaltegger, U., and Blackburn, T. J.: Correlating the end-Triassic mass extinction and flood basalt volcanism at the 100,000-year level, Geology, 38, 387–390, 2010.

Schrag, D. P.: Control of atmospheric CO$_2$ and climate through Earth history, Geochim. Cosmochim. Acta, 66, p. A688, 2002.

Schrag, D. P., Berner, R. A., Hoffman, P. F., and Halverson, G. P.: On the initiation of a snowball Earth, Geochem. Geophy. Geosy., 3, doi:10.1029/2001GC000219, 2002.

Self, S., Thordarson, T., and Widdowson, M.: Gas fluxes from flood basalt eruptions, Elements, 1, 283–287, 2005.

Selverstone, J. and Gutzler, D. S.: Post-125 Ma carbon storage associated with continent-continent collision, Geology, 21, 885–888, 1993.

Seton, M., Gaina, C., Muller, R. D., and Heine, C.: Mid-Cretaceous seafloor spreading pulse: Fact or fiction?, Geology, 37, 687–690, 2009.

Shackleton, N. J.: The carbon isotope record of the Cenozoic: history of organic carbon burial and of oxygen in the ocean and atmosphere, Special Publications, Geol. Soc. London, 26, 423–434, 1987.

Smith, A. G. and Hallam, A.: The fit of the southern continents, Nature, 225, 139–144, 1970.

Smith, M. E., Carroll, A. R., and Mueller, E. R.: Elevated weathering rates in the Rocky Mountains during the Early Eocene Climatic Optimum, Nat. Geosci., 1, 370–374, 2008.

Srivastava, S. P. and Tapscott, C. R.: Plate kinematics of the North Atlantic, in: The Geology of North America, The Western North Atlantic Region, edited by: Tucholke, B. E. and Vogt, P. R., Geological Society of America, Boulder, 379–404, 1986.

Staudigel, H., Hart, S. R., Schmincke, H.-U., and Smith, B. M.: Cretaceous ocean crust at DSDP Sites 417 and 418: Carbon uptake from weathering versus loss by magmatic outgassing, Geochim. Cosmochim. Acta, 53, 3091–3094, 1989.

Staudigel, H., Hart, S. R., Schmincke, H.-U., and Smith, B. M.: Reply to "Global CO$_2$ degassing and the carbon cycle": A Comment by R. A. Berner, Geochim. Cosmochim. Acta, 54, 2891, 1990a.

Staudigel, H., Hart, S. R., Schmincke, H.-U., and Smith, B. M.: Reply to R. A. Berner's response, Geochim. Cosmochim. Acta, 54, 2893, 1990b.

Stickley, C. E., Brinkhuis, H., Shellenberg, S. A., Sluijs, A., Rohl, U., Fuller, M., Grauert, M., Huber, M., Warnaar, J., and Williams, G. L.: Timing and nature of the deepening of the Tasmanian Gateway, Paleoceanography, 19, PA4027, doi:4010.1029/2004PA001022, 2004.

Tejada, M. L. G., Suzuki, K., Kuroda, J., Coccioni, R., Mahoney, J. J., Ohkouchi, N., Sakamoto, T., and Tatsumi, Y.: Ontong Java Plateau eruption as a trigger for the early Aptian oceanic anoxic event, Geology, 37, 855–858, 2009.

Tera, F., Brown, L., Morris, J., Sacks, I. S., Klein, J., and Middleton, R.: Sediment incorporation in island-arc magmas: Inferences from ^{10}Be, Geochim. Cosmochim. Acta, 50, 535–550, 1986.

Thomas, D. J. and Bralower, T. J.: Sedimentary trace element constraints on the role of North Atlantic Igneous Province volcanism in late Paleocene-early Eocene environmental change, Mar. Geol., 217, 233–254, 2005.

Volk, T.: Sensitivity of climate and atmospheric CO_2 to deep-ocean and shallow-ocean carbonate burial, Nature, 337, 637–640, 1989.

Volk, T. and Hoffert, M. I.: Ocean carbon pumps: Analysis of relative strengths and efficiencies in ocean-driven atmospheric $C0_2$ changes, Am. Geophys. Union Monogr., 32, 99–110, 1985.

Walker, J. C. G., Hays, P. B., and Kasting, J. F.: A negative feedback mechanism for the long-term stabilization of Earth's surface-temperature, J. Geophys. Res.-Atmos., 86, 9776–9782, 1981.

West, A. J., Bickle, M. J., Collins, R., and Brasington, J.: Small-catchment perspective on Himalayan weathering fluxes, Geology, 30, 355–358, 2002.

West, A. J., Galy, A., and Bickle, M.: Tectonic and climatic controls on silicate weathering, Earth Planet. Sc. Lett., 235, 211–228, 2005.

Wilkinson, B. H. and Walker, J. C. G.: Phanerozoic cycling of sedimentary carbonate, Am. J. Sci., 289, 525–548, 1989.

Wilson, P. A., Norris, R. D., and Cooper, M. J.: Testing the Cretaceous greenhouse hypothesis using glassy foraminiferal calcite from the core of the Turonian tropics on Demerara Rise, Geology, 30, 607–610, 2002.

Wright, J. D., Miller, K. G., and Fairbanks, R. G.: Early and Middle Miocene stable isotopes: Implications for deepwater circulation and climate, Paleoceanography, 7, 357–389, 1992.

Yang, Z. and Besse, J.: Paleomagnetic study of Permian and Mesozoic sedimentary rocks from Northern Thailand supports the extrusion model for Indochina, Earth Planet. Sc. Lett., 117, 525–552, 1993.

Yang, Z., Yin, J., Sun, Z., Otofuji, Y.-I., and Sato, K.: Discrepant Cretaceous paleomagnetic poles between Eastern China and Indochina: a consequence of the extrusion of Indochina, Tectonophysics, 334, 101–113, 2001.

Yin, A. and Harrison, T. M.: Geologic evolution of the Himalayan–Tibetan Orogen, Annu. Rev. Earth Planet. Sci., 28, 211–280, 2000.

You, Y., Huber, M., Muller, R. D., Poulsen, C. J., and Ribbe, J.: Simulation of the Middle Miocene Climate Optimum, Geophys. Res. Lett., 36, L04702, doi:10.1029/2008GL036571, 2009.

Zachos, J., Pagani, M. N., Sloan, L., Thomas, E., and Billups, K.: Trends, rhythms, and aberrations in global climate 65 Ma to Present, Science, 292, 686–693, 2001.

Zanchi, A., Zanchetta, S., Garzanti, E., Balini, M., Berra, F., Mattei, M., and Muttoni, G.: The Cimmerian evolution of the Nakhlak–Anarak area, Central Iran, and its bearing for the reconstruction of the history of the Eurasian margin, Special Publications, Geol. Soc. London, 312, 261–286, 2009.

Zhu, B., Kidd, W. S. F., Rowley, D. B., Currie, B. S., and Shafique, N.: Age of initiation of the India–Asia collision in the east-central Himalaya, J. Geol., 113, 265–285, 2005.